using the BLAT search program. This showed that 99.1% of the ESTs (287 849 reads) mapped to the human genome (Table 4). This mapping result was filtered further using the UCSC Genome Browser and a pslCDnaFilter. Finally, 93.2% (270 673 reads) of the marmoset ESTs were assigned specifically and exactly to the human genome.

The nucleotide sequence identity between aligned sequences was calculated after each EST had been mapped to the genome (Supplementary Fig. S2). The majority of ESTs shared 90–96% identity with the human genome. The relatively low identity between the ESTs and human sequences was analogous to the identity between the EST and Refseq shown in Table 3. It should be noted that the degree of mapping to the human genome did not differ significantly among the five cDNA libraries (data not shown).

3.3.1. ESTs that were mapped to exonic regions of the human genome The CAP3 method identified 17 232 contigs (Table 1). The contig sequences represented those that were read multiple times in the overlapping regions and they were considered more reliable than single-read singletons. These 17 232 contigs were mapped onto the human genome according to the filtering method shown in Table 4. Furthermore, information from human Refseqs was used to determine whether the mapped contigs corresponded to exonic sequences of the human gene. This approach identified 15 089 contigs (88% of 17 232) that mapped onto the human genome and that corresponded to human Refseqs. These 15 089 contigs, which consisted of 218 857 ESTs, were considered to be representative of the genes that are commonly transcribed in marmosets and humans.

Of these 15 089 contigs, ESTs that were present in only one type of cDNA library were identified. Of these tissue-specific contigs, those with the highest numbers of constitutive ESTs are shown in Table 5. The contigs with >1000 ESTs were *ALB*, *HPR*, *ORM2*, and *ORM1* from MLI, and *PRM1* from MTE. Most of the genes listed in Table 5 are known to be characteristic of each specific cell type/tissue.

3.3.2. ES cell-specific transcripts Supplementary Table S2 shows previously reported cDNA/EST studies of primates other than the marmoset.[20–24] These species include *Pan troglodytes*, *Macaca fascicularis*, and *Chlorocebus sabaeus*, while the tissues included the brain, skin, liver, B lymphocytes, bone marrow, pancreas, spleen, thymus, and peripheral blood mononuclear cells. As the current study is the first example of the use of monkey-derived ES cells in EST studies, the ES-specific transcripts are mentioned briefly (see Supplementary Table S3 where the contigs containing >5 ESTs are listed).

The most notable were *LIN28A*, *NANOG*, and *SOX2* because, together with *OCT4*, they are known to reprogram human somatic cells to induced pluripotent stem cells.[25] *LIN28A* and *NANOG* contribute to the maintenance of pluripotency in stem cells.[26–28]

Table 4. Mapping of ESTs on the human genome

Libraries	Number of marmoset ESTs	Number of ESTs mapped on the human genome (raw data)	Number of ESTs mapped on the human genome (filtered)
MES	71 009	70 375	66 894 (94.2%)
MLI	56 232	55 602	52 405 (93.2%)
MSC	29 258	28 931	27 253 (93.1%)
MSP	61 831	61 300	58 170 (94.1%)
MTE	72 096	71 641	65 951 (91.5%)
All	290 426	287 849 (99.1%)	270 673 (93.2%)

Marmoset ESTs (290 426) were mapped on the human genome (hg19) by using a BLAT search program (−stepSize = 5, −minScore = 50, −minIdentity = 80, −repMatch = 2253). This initial mapping gave a number of 287 849 (99.1%) ESTs. These ESTs were then filtered, following a UCSC Genome Browser and using a pslCDnaFilter (−minId = 0.85, −minCover = 0.75, −globalNearBest = 0.0025, −minQSize = 20, −minNonRepSize = 16, −ignoreNs, −bestOveralp). Basis for adopting this filtering condition was as follows. A use of the condition such as (−minId = 0.95, −minCover = 0.25) selected only 159 309 ESTs (54.9%), indicating −minId = 0.95 to be extremely strict in the exactness. Therefore, we lowered the −minId to 0.85 (and −minCover = 0.25) and found the reasonably selected numbers of exact ESTs. Thus, under this −minId of 0.85, we then tried to improve the specificity by increasing −minCover to 0.75 (since 0.90 appeared too strict, 0.90 was not used). This −minCover number of 0.75 is roughly equal to the expected coverage of coding sequence [the average length of EST was 619 nt, and the average length of 5′UTR of human transcripts is 170 nt, therefore, an expected coverage between coding sequences and ESTs would be (619−170)/619 = 0.73]. Eventually, a condition of −minId = 0.85, −minCover = 0.75 filtered 270 673 ESTs (93.2%) as exact and specific.

Table 5. Top five genes expressed abundantly in each cDNA library

Libraries	Gene symbols	Descriptions	Number of ESTs
MES	*PYY*	Peptide YY	123
MES	*LIN28A*	Lin-28 homologue A	50
MES	*C6orf221*	Chromosome 6 open reading frame 221	46
MES	*NANOG*	Nanog homeobox	45
MES	*ERVMER34-1*	Endogenous retrovirus group MER34, member 1	28
MLI	*ALB*	Albumin	4492
MLI	*HPR*	Haptoglobin-related protein	1537
MLI	*ORM2*	Orosomucoid 2	1227
MLI	*ORM1*	Orosomucoid 1	1221
MLI	*APOA2*	Apolipoprotein A-II	673
MSC	*SNAP25*	Synaptosomal-associated protein, 25 kDa	109
MSC	*PLP1*	Proteolipid protein 1	58
MSC	*CALCA*	Calcitonin-related polypeptide alpha	51
MSC	*STMN2*	Stathmin-like 2	30
MSC	*THY1*	Thy-1 cell surface antigen	28
MSP	*MS4A1*	Membrane-spanning 4-domains, subfamily A, member 1	62
MSP	*ITGB2*	Integrin, beta 2	29
MSP	*HLA-DPA1*	Major histocompatibility complex, class II, DP alpha 1	26
MSP	*CLEC4F*	C-type lectin domain family 4, member F	20
MSP	*CD53*	CD53 molecule	18
MTE	*PRM1*	Protamine 1	1,198
MTE	*TNP1*	Transition protein 1	161
MTE	*HMGB4*	High mobility group box 4	139
MTE	*PHF7*	PHD finger protein 7	138
MTE	*DKKL1*	Dickkopf-like 1	107

Shown are the contigs that were detected only in one out of five cDNA libraries and possessed larger numbers of constituting ESTs.

C6orf221 (also known as *ECAT1*, ES cell-associated transcript 1) and *DPPA5* belong to the same gene family, and they are expressed specifically in human ES cells.[29,30] The frequent appearance of the claudin family (see *CLDN6*, *CLDN9*, *CLDN7*, and *CLDN4*) was also noted, although its biological significance is not known.

3.3.3. ESTs that were mapped onto the human genome outside exonic regions We noted that there was another category of contigs that was mapped onto the human genome, but not located in exonic regions (i.e. contigs that shared no homology with human Refseqs). These comprised 808 contigs (4.7% of 17 232) with 5578 ESTs. These 808 contigs represented transcribed genes in the marmoset. Although they were conserved in the human genome, they did not appear to be transcribed as genes; hence, they were not characterized as human genes.

Next, the number of marmoset cDNA libraries, in which each contig was expressed, was determined. The number of contigs with ESTs detected in libraries 1 (i.e. only MES), 2 (i.e. MES and MTE), 3, 4, and 5 (all of MES, MLI, MSC, MSP, and MTE) were 562, 195, 28, 7, and 6, respectively (808 in total). Of the 562 contigs, 29 were found in MES, 31 in MLI, 28 in MSC, 87 in MSP, and 387 in MTE (562 in total). It appeared that the genes expressed in the marmoset testes (387/562 = 69%) had an increased likelihood of not being expressed in humans compared with the genes expressed in other tissues (31%/4 = 7.8%).

Supplementary Table S4 shows the 20 contigs whose constituting ESTs' numbers were the largest among the 808 contigs. Interestingly, the five contigs that had the highest numbers of ESTs (ID: 198, 15591, 1258, 1567, and 3721) also had ESTs in all five libraries. In the previous paragraph, it was noted that six contigs were expressed in all five libraries. It was found that five out of these six contigs were widely expressed at a high level in the marmoset. This suggests that actively expressed genes in the marmoset may even be non-transcribed as genes in humans. Many of the remaining genes in Supplementary Table S4 were expressed in a combination of tissues e.g. MLI and MSP, or MLI and MSC, or only in MTE.

3.3.4. Characterization of 808 contigs in non-coding RNA or silent regions of the human genome The 808 contigs described above were mapped onto the human genome, but did not have any corresponding human Refseqs. The human genome browser at UCSC also supports mapping of RNA-seq and large intergenic non-coding RNAs (linc RNA).[31,32] The locations of these RNA-seq/linc RNAs were checked in relation to the marmoset ESTs mapped onto the human genome. The tissues that are used in common in RNA-seq/linc RNA studies[31,32] and the current study are the liver, brain, and testis; hence, 138 contigs expressed in MLI, 125 in MSC, and 516 in MTE (total 779) were used for the analyses (Supplementary Table S5). This showed that 500 contigs (64% of 779) matched RNA-seqs, while 98 contigs had corresponding sequences in RNA-seq and linc RNA. However, 259 contigs (33% of 779) did not have any counterparts in RNA-seq or linc RNA, suggesting that they were not expressed as RNA.

In summary, of the 808 contigs that did not have a corresponding human Refseq, two-thirds were probably expressed as non-coding RNA, whereas the other third appeared to be silent. This potentially suggests that these 808 may have lost their characteristics as genes during human evolution.

3.3.5. Identification of so far unknown genes based on probable full-length cDNA sequences The degree of conservation and/or divergence in marmoset and human genes was analysed using the following approach as well. Supplementary Fig. S3A shows a flow chart of the method used for selecting 'unknown genes.' First, getorf in EMBOSS was applied to extract 60 568 unigenes (see Table 1 where 60 568 represents the sum of contigs and singlets). Thus, sequences were selected that contain an open-reading frame spanning an initiating methionine through to a stop codon, with a poly(A) tail at the 3′ end. The G-cap was preserved in most ESTs, so the selected sequences probably represented 'full-length' cDNAs. This approach selected 3151 unigenes.

Each unigene was mapped onto the human genome. In total, 2595 sequences were mapped onto the human genome. Of the 556 marmoset sequences that could not be mapped onto the human genome, 127 were annotated and identified using the Refseq information of all living species, while 311 (306 + 5) shared homology with sequences registered in EST/nr sequence databases. The remaining 118 unigenes could not be annotated, suggesting that they represent potentially unknown genes.

Notably, only 1 sequence was derived from MLI and MSC, 3 from MSP, 14 from MES, while 104 from MTE. This might indicate comparatively abundant expression of unknown genes in the marmoset testis. The length of the polypeptides encoded by the 'unknown genes' ranged from 11 to 131 amino acids, with an average of 47 (Supplementary Fig. S4). It should be noted that no known domains/motifs were detected in these 'unknown' amino acid sequences using the INTERPRO program.

3.3.6. Further characterization of the 118 'unknown genes' It is possible that the 118 genes with ORFs might not encode polypeptides but may represent non-coding RNAs. In fact, five shared homology (1e-5) with non-coding RNAs in a comprehensive database (http://www.ncrna.org/frnadb/) and a marmoset-derived non-coding RNA database (ftp://ftp.ensembl.org/pub/release 70/fasta/callithrix_jacchus/ncrna/). Furthermore, 66 out of 118 genes could be aligned with the human genome if a 75% sequence similarity was employed, and each of these alignments covered more than half of each sequence. Therefore, a significant portion of the 118 genes had features of both polypeptide-coding genes and non-coding RNAs. Supplementary Fig. S3B and its legend provide further details on the unbiased approach used to identify unknown genes.

3.4. Availability of the resources

A Web server of marmoset cDNAs has been constructed (http://marmoset.nig.ac.jp/index.html), in which each marmoset EST sequence is mapped onto the human genome. Information accessible via the human genome browser can be obtained on this server, including the Ensembl gene annotation, Refseqs, and RNA-seq/linc RNA. This Web server can be used as a search engine, so the marmoset EST sequences can be BLASTed and the results displayed. The cDNAs libraries and/or the clones are available upon request from the DNA Bank, RIKEN BioResource Center (RDB no. 6388–6392). These deposited resources are expected to be valuable for future studies that use the common marmoset as an experimental animal model.

Acknowledgements: S.T. and M.S. are very grateful to Atsushi Toyoda (National Institute of Genetics, Mishima, Japan) for his continuous encouragement, which helped us to accomplish this work. We thank members of Sequence Technology Team, RIKEN Genomic Sciences Center for the generation of marmoset ESTs.

Supplementary data: Supplementary Data are available at www.dnaresearch.oxfordjournals.org.

Funding

Sequencing work was supported by a Special Fund for RIKEN Genomic Sciences Center.

References

1. Mansfield, K. 2003, Marmoset models commonly used in biomedical research, *Comp. Med.*, **53**, 383–92.
2. Massacesi, L., Genain, C., Lee-Parritz, D., et al. 1995, Active and passively induced experimental autoimmune encephalomyelitis in common marmosets: a new model for multiple sclerosis, *Ann. Neurol.*, **37**, 519–30.
3. Genain, C. and Hauser, S. 2001, Experimental allergic encephalomyelitis in the new world monkey Callithrix jacchus, *Immunol. Rev.*, **183**, 159–92.
4. 't Hart, B., Laman, J., Bauer, J., et al. 2004, Modeling of multiple sclerosis: lessons learned in a non-human primate, *Lancet Neurol.*, **3**, 588–97.

5. Sasaki, E., Suemizu, H., Shimada, A., et al. 2009, Generation of transgenic nonhuman primates with germline transmission, *Nature*, **459**, 515–6.
6. Izawa, K., Tani, K., Nakazaki, Y., et al. 2004, Hematopoietic activity of common marmoset CD34 cells isolated by a novel monoclonal antibody MA24, *Exp. Hematol.*, **32**, 843–51.
7. Ito, R., Maekawa, S., Kawai, K., et al. 2008, Novel monoclonal antibodies recognizing different subsets of lymphocytes from the common marmoset (Callithrix jacchus), *Immunol. Lett.*, **121**, 116–22.
8. Kametani, Y., Suzuki, D., Kohu, K., et al. 2009, Development of monoclonal antibodies for analyzing immune and hematopoietic systems of common marmoset, *Exp. Hematol.*, **37**, 1318–29.
9. Brok, H., Hornby, R., Griffiths, G., et al. 2001, An extensive monoclonal antibody panel for the phenotyping of leukocyte subsets in the common marmoset and the cotton-top tamarin, *Cytometry*, **45**, 294–303.
10. Kohu, K., Yamabe, E., Matsuzawa, A., et al. 2008, Comparison of 30 immunity-related genes from the common marmoset with orthologues from human and mouse, *Tohoku J. Exp. Med.*, **215**, 167–80.
11. Sasaki, E., Hanazawa, K., Kurita, R., et al. 2005, Establishment of novel embryonic stem cell lines derived from the common marmoset (*Callithrix jacchus*), *Stem Cells*, **23**, 1304–13.
12. Ohtake, H., Ohtoko, K., Ishimaru, Y., and Kato, S. 2004, Determination of the capped site sequence of mRNA based on the detection of cap-dependent nucleotide addition using an anchor ligation method, *DNA Res.*, **11**, 305–9.
13. Altschul, S.F., Gish, W., Miller, W., et al. 1990, Basic local alignment search tool, *J. Mol. Biol.*, **215**, 403–10.
14. Kent, W.J. 2002, BLAT—the BLAST-like alignment tool, *Genome Res.*, **12**, 656–64.
15. Li, W. and Godzik, A. 2006, Cd-hit: a fast program for clustering and comparing large sets of protein or nucleotide sequences, *Bioinformatics*, **22**, 1658–9.
16. Huang, X. and Madan, A. 1999, CAP3: a DNA sequence assembly program, *Genome. Res.*, **9**, 868–77.
17. Ewing, B. and Green, P. 1998, Base-calling of automated sequencer traces using phred. II. Error probabilities, *Genome. Res.*, **8**, 186–94.
18. Rice, P., Longden, I. and Bleasby, A. 2000, EMBOSS: the European Molecular Biology Open Software Suite, *Trends in Genet.*, **16**, 276–7.
19. Quevillon, E., Silventoinen, V., Pillai, S., et al. 2005, InterProScan: protein domains identifier, *Nucleic Acids Res.*, **33**, 116–20.
20. Sakate, R., Osada, N., Hida, M., et al. 2003, Analysis of 5′-end sequences of chimpanzee cDNAs, *Genome. Res.*, **13**, 1022–6.
21. Chen, W.H., Wang, X.X., Lin, W., et al. 2006, Analysis of 10,000 ESTs from lymphocytes of the cynomolgus monkey to improve our understanding of its immune system, *BMC Genomics*, **7**, 82.
22. Uno, Y., Suzuki, Y., Wakaguri, H., et al. 2008, Expressed sequence tags from cynomolgus monkey (*Macaca fascicularis*) liver: a systematic identification of drug-metabolizing enzymes, *FEBS Lett.*, **582**, 351–8.
23. Osada, N., Hirata, M., Tanuma, R., et al. 2009, Collection of *Macaca fascicularis* cDNAs derived from bone marrow, kidney, liver, pancreas, spleen, and thymus. *BMC Res. Notes*, **2**, 199.
24. Tchitchek, N., Jacquelin, B., Winker, P., et al. 2012, Expression sequence tag library derived from peripheral blood mononuclear cells of the chlorocebus sabaeus, *BMC Genomics*, **13**, 279.
25. Yu, J., Vodyanik, M.A., Smuga-Otto, K., et al. 2007, Induced pluripotent stem cell lines derived from human somatic cells, *Science*, **318**, 1917–20.
26. Mitsui, K., Tokuzawa, Y., Itoh, H., et al. 2003, The homeoprotein Nanog is required for maintenance of pluripotency in mouse epiblast and ES cells, *Cell*, **113**, 631–42.
27. Darr, H. and Benvenisty, N. 2009, Genetic analysis of the role of the reprogramming gene *LIN-28* in human embryonic stem cells, *Stem Cells*, **27**, 352–62.
28. Xu, B., Zhang, K. and Huang, Y. 2009, Lin28 modulates cell growth and associates with a subset of cell cycle regulator mRNAs in mouse embryonic stem cells, *RNA*, **15**, 357–61.
29. Kim, S.K., Suh, M.R., Yoon, H.S., et al. 2005, Identification of developmental pluripotency associated 5 expression in human pluripotent stem cells, *Stem Cells*, **23**, 458–62.
30. Pierre, A., Gautier, M., Callebaut, I., et al. 2007, Atypical structure and phylogenomic evolution of the new eutherian oocyte- and embryo-expressed *KHDC1/DPPA5/ECAT1/OOEP* gene family, *Genomics*, **90**, 583–94.
31. Wang, E.T., Sandberg, R., Luo, S., et al. 2008, Alternative isoform regulation in human tissue transcriptomes, *Nature*, **456**, 470–6.
32. Cabili, M.N., Trapnell, C., Goff, L., et al. 2011, Integrative annotation of human large intergenic noncoding RNAs reveals global properties and specific subclasses, *Genes Dev.*, **25**, 1915–27.

This article has been accepted for publication in a future issue of this journal, but has not been fully edited. Content may change prior to final publication. Citation information: DOI 10.1109/JBHI.2013.2286155, IEEE Journal of Biomedical and Health Informatics

Automated Estimation of Fetal Cardiac Timing Events from Doppler Ultrasound Signal Using Hybrid models

Faezeh Marzbanrad, *Student Member, IEEE,* Yoshitaka Kimura, Kiyoe Funamoto, Rika Sugibayashi, Miyuki Endo, Takuya Ito, Marimuthu Palaniswami, *Fellow, IEEE,* and Ahsan H Khandoker*, *Senior Member, IEEE*

***Abstract*—In this paper a new noninvasive method is proposed for automated estimation of fetal cardiac intervals from Doppler Ultrasound (DUS) signal. This method is based on a novel combination of Empirical Mode Decomposition (EMD) and hybrid support vector machines - Hidden Markov Models (SVM/HMM). EMD was used for feature extraction by decomposing the DUS signal into different components (IMFs), one of which is linked to the cardiac valve motions, i.e. opening (o) and closing (c) of the Aortic (A) and Mitral (M) valves . The non-invasive fetal electrocardiogram (fECG) was used as a reference for the segmentation of the IMF into cardiac cycles. The hybrid SVM/HMM was then applied to identify the cardiac events, based on the amplitude and timing of the IMF peaks as well as the sequence of the events. The estimated timings were verified using pulsed doppler images. Results show that this automated method can continuously evaluate beat-to-beat valve motion timings and identify more than 91% of total events which is higher than previous methods. Moreover the changes of the cardiac intervals were analysed for three fetal age groups: 16-29, 30-35 and 36-41 weeks. The time intervals from Q-wave of fECG to Ac (Systolic Time Interval, STI), Ac to Mo (Isovolumic Relaxation Time, IRT), Q-wave to Ao (Pre-ejection Period, PEP) and Ao to Ac (Ventricular Ejection Time, VET) were found to change significantly ($p < 0.05$) across these age groups. In particular, STI, IRT and PEP of the fetuses with 36-41 week were significantly ($p < 0.05$) different from other age groups. These findings can be used as sensitive markers for evaluating the fetal cardiac performance.**

***Index Terms*—Doppler Ultrasound, Fetal cardiac intervals, Fetal monitoring, Empirical Mode Decomposition (EMD), Support Vector Machine (SVM), Hidden Markov Models (HMM), Hybrid SVM/HMM.**

I. Introduction

EACH year 1 out of 125 babies is born with Congenital Heart Disease (CHD) [1]. Prenatal CHD has even around 10-fold higher incidence, since a majority of these defects end in intrauterine death [2]. Even with the improved treatment options that are now available, every fifth child with CHD dies during the first year of life. The mortality rate correlates closely with the severity of the heart defect and its early clinical manifestations. By diagnosing these conditions prenatally, it may be possible to reduce perinatal morbidity and mortality [3]. Furthermore, it provides tremendous medical, psychological, and economical benefits [4].

Various antenatal fetal assessment techniques have been advocated to evaluate antepartum fetal risks. Fetal circulation is one of the main concerns in fetal assessment which has a crucial importance, especially the evaluation of the heart action may give more useful information about the fetus in the antenatal period [5]. Fetal Heart Rate (FHR) monitoring is commonly used for this purpose and usually performed by using Cardiotocography (CTG) which is a combination of Doppler Ultrasound (DUS) and measured uterine activity.

However, FHR monitoring is not enough for a thorough assessment of the fetal state. There are more sensitive markers for assessing the cardiac performance which are illustrated in figure 1. By these markers the electromechanical coupling of the heart is evaluated, which is a fundamental and clinically significant part of the heart physiology [6], [7]. The opening and closure timings of the cardiac valves are the main bases for estimating these electromechanical indices [8]. Among these markers the Systolic Time Intervals (STI) have received considerable attention as indicators of myocardial function. From a clinical standpoint, Pre-Ejection Period (PEP), Isovolumetric Contraction Time (ICT) and left Ventricular Ejection Time (VET)are the most useful of STIs [8]. For example, PEP

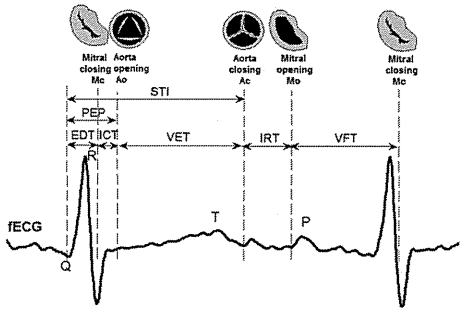

Fig. 1. An illustrative example of fetal cardiac intervals: Systolic time interval (STI), Electromechanical Delay Time (EDT), Isovolumic Contraction Time(ICT), Preejection Period (PEP), Ventricular Ejection Time (VET), Isovolumic Relaxation Time (IRT), Ventricular Filling Time (VFT).

* Corresponding author

F. Marzbanrad, M. Palaniswami and AH. Khandoker are with the Electrical and Electronic Engineering Department, University of Melbourne, Melbourne, VIC 3010, Australia (e-mail:f.marzbanrad@student.unimelb.edu.au, palani@unimelb.edu.au, ahsank@unimelb.edu.au).

A. Khandoker is also with Biomedical Engineering Department, Khalifa University of Science, Technology and Research, Abu Dhabi, UAE (phone: +971-(0)2-5018559, e-mail: ahsan.khandoker@kustar.ac.ae).

Y. Kimura, K. Funamoto, R. Sugibayashi, M. Endo and T. Ito are with Graduate School of Medicine, Tohoku University, Sendai, Japan.

(e-mail: ykimura@med.tohoku.ac.jp, kiyoe_konnofunamoto@med.tohoku.ac.jp, rikasugiba@gmail.com, miyukien@med.tohoku.ac.jp, i-takuya@med.tohoku.ac.jp).

This article has been accepted for publication in a future issue of this journal, but has not been fully edited. Content may change prior to final publication. Citation information: DOI 10.1109/JBHI.2013.2286155, IEEE Journal of Biomedical and Health Informatics

is reported as a sensitive indicator of the function state of the fetal myocardium and it becomes prolonged early in the development of hypoxemia and acidosis [8]. Another study suggested to use ICT as a reliable index which can be substituted for fetal cardiac contractility [9]. Other cardiac intervals are also valuable for clinical applications [8], [10]. Several methods have been proposed for obtaining these intervals.

Fetal echocardiography is a technique which can visualize different parts of the heart structure as well as the blood flow through the valves. However it is an expensive method and only particular maternal and fetal conditions indicate the need for it. Furthermore, in most cases, primary care physicians or obstetricians cannot appropriately analyze the heart views and only qualified individuals can perform this highly specialized examination [11]. Due to these problems simpler and more accurate alternative methods have been investigated.

Starting in 1980s, a number of non-invasive methods have been proposed which mainly aimed to analyze the systolic time intervals by using the abdominal ECG and the DUS signal [12]–[15]. Band pass filter was used in these methods for filtering the DUS signal, after which the cardiac events were identified manually. The major problem with these methods is the highly variability of the DUS signal over time as well as the poor quality of the abdominal ECG.

In 2001, Koga et. al. used the digital narrow band-pass filter to divide the DUS signal into different frequency shift ranges. The mitral and aortic valve motions were then identified from the peaks in one of the filtered signals [15].

With the improved signal processing techniques and more powerful processors over the last decade, the information content of the DUS signal has been acquired more easily. In 2001, Shakespeare et. al. proposed a method in which the DUS signal was analyzed by the Short Time Fourier Transform (STFT) [16]. They have shown that the high frequency component of the DUS signal is linked to the valve movements, while the low frequency one is associated with the cardiac wall motion. They also demonstrated the variability of the content of the DUS data on a beat-to-beat basis.

A common issue which is noticed in all of these studies is the transient nature of the DUS signal as well as the wide changes in the signal content and spectral characteristics. Therefore another method was recently proposed which applied the multi-resolution wavelet analysis to the DUS signal [17]. Wavelet analysis is a powerful method for decomposing non-stationary signals with variable spectral characteristic over time. Using wavelet analysis, the DUS signal is decomposed into different scales with resolution levels. As shown in [17], valve movements were visualized as peaks in the detailed signal at level 2 wavelet decomposition. Each peak was then manually assigned to be linked to the opening and closure of the cardiac valves. Since the abdominal ECG is noisy and it is difficult to observe the fetal R-wave, the extracted fECG was used, which was separated from the abdominal ECG mixture using blind source separation with reference [18]. Furthermore the correlation of the cardiac cycle length (R-R interval) with the interval of the R wave to each valve motion was investigated which has potential clinical applications. This correlation was found to be more significant for the abnormal cases and it was introduced as a criterion for diagnosing fetal heart abnormalities. Automatic identification of these abnormalities was investigated in their next studies [19], [20]. Based on the current methods, fetal cardiac valve movements can be recognized manually from a high frequency component of the DUS signal. However, DUS is usually corrupted by noise and interferences and it is also sensitive to the position of the fetus and the transducer. Therefore current methods which are based on manual recognition may not be practical and reliable. Thus an automated approach is proposed in this paper, to identify the occurrence of the cardiac events based on the pattern, timings and sequence of the valve and wall movements in the DUS signal components.

In this paper, instead of STFT or the wavelet analysis, it is proposed to use Empirical Mode Decomposition (EMD) because it is a data-driven algorithm which is used for decomposing nonlinear and non-stationary time series [21]. It has been used extensively in many different applications, such as: speech processing, image processing and biomedical signal processing [22]–[26]. EMD has been also used for better estimation of the fetal heart rate, using Ultrasound Doppler signal [27], [28]. Three approaches are introduced to be combined with EMD for automated identification: Hidden Markov Model (HMM), Support Vector Machine (SVM) and hybrid SVM/HMM. The hybrid method has been originally proposed for speech processing applications [29], [30] and to our best knowledge, it has never been used in this application. Furthermore the changes of the cardiac intervals from the 16th to 41th week of gestation were evaluated in this paper.

II. Methods

A. Subjects

Simultaneous recordings of the abdominal ECG signals and Doppler ultrasound signals from 45 pregnant women at the gestational age of 16 to 41 weeks with normal single pregnancies were collected from Tohoku University Hospital in Japan. A total of 45 recordings (each of 1 minute length) were sampled at 1 kHz with 16-bit resolution. All 45 subjects were divided into three age groups for analysis: 16-29 weeks, 30-35 weeks and 36-41 weeks, including 15, 12 and 18 fetuses, respectively. The study protocol was approved by Tohoku University Institutional Review Board and written informed consent was obtained from all subjects. The continuous DUS data were obtained using Ultrasonic Transducer 5700 (fetal monitor 116, Corometrics Medical Systems Inc.) with 1.15 MHz signals. To compare the actual appearance of the aortic valve's opening and closing pattern with valve timing events appeared in DUS signals, pulsed-wave Doppler signals were obtained from convex 3.5 Hz of HITACHI ultrasound scanner (Ultrasonic diagnostic instrument Model EUB-525; HITACHI health medical corporation). The detailed procedure for experimental set up and transabdominal ECG data collection was described in our previous study [18]. FECG signals were extracted from the composite abdominal signal using a method that combines cancelation of the mother's ECG signal and the blind source separation with the reference signal (BSSR) as described in our earlier study [18] and summarized as

This article has been accepted for publication in a future issue of this journal, but has not been fully edited. Content may change prior to final publication. Citation information: DOI 10.1109/JBHI.2013.2286155, IEEE Journal of Biomedical and Health Informatics

follows.The electrical activities of the heart form a vector in the direction of excitation which is called the heart vector [31]. The cancelation of the maternal ECG component was performed by subtracting the linear combination of mutually orthogonal projections of the heart vector. After removing maternal ECG, BSSR, which is a kind of neural network methods, extracted fetal ECG signals from complex mixed signals using DUS signal as the reference [18].

B. Empirical Mode Decomposition (EMD)

One of the main methods used in this paper is Empirical Mode Decomposition (EMD) which was first introduced by Huang et al. [21]. It is a single channel method for decomposing a complicated signal into a set of different oscillatory modes. These components are called Intrinsic-Mode functions (IMF) and are zero mean, orthogonal and spectrally independent. The IMFs do not necessarily have constant frequency or amplitude.

EMD is an empirical procedure which is defined only by an algorithm and basically does not focus on any analytical formulation for theoretical analysis. It has been used extensively in image, speech and audio processing applications as well as biomedical signal processing [22]–[26] where its effectiveness is shown.

In brief, the EMD adaptively decomposes a signal into the IMFs through a specific algorithm which is called "sifting procedure". Therefore for each mode, the highest frequency component is locally extracted out of the input signal.

The sifting process is based on two constraints:

1. The number of zero crossing and extrema in the whole data must be the same or at most differ by one.
2. At each point, the mean value of the upper and lower envelopes which are constructed based on the local maxima and minima is zero.

The sifting algorithm begins with identifying local maxima and minima of the signal to be decomposed. Then the local maxima and minima are interpolated to find the upper and lower envelopes respectively. Then the mean of these two envelopes is subtracted from the signal. The process is repeated for the residue until it meets a stoppage criteria which limits the size of the standard deviation computed for two consecutive residues. The first IMF is then obtained from the residue of the final subtraction. The whole procedure is performed on the residue of this IMF to find the second IMF. This process continues to obtain all IMFs and the final residue has zero or one extrema. More details can be found in [21].

EMD can be used for analyzing nonlinear and non-stationary signals. It is a data driven algorithm which is able to decompose the signal in a natural approach and doesn't need any prior information about the component of interest. Therefore in this paper it is proposed to apply EMD to the DUS signal to decompose it to the IMFs which naturally have different frequency bands. An example of Applying EMD to the DUS data is shown in Figure 2. As discussed in the next sections, the peaks of the envelope of the first IMF provide the features for identification of the cardiac events.

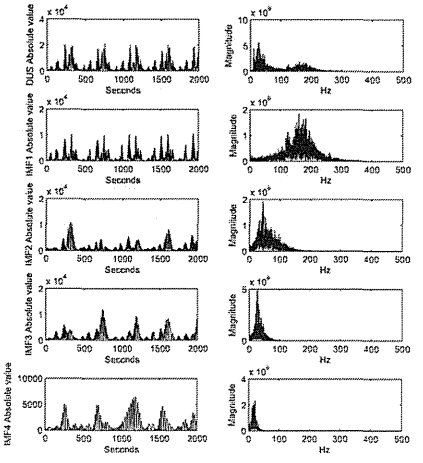

Fig. 2. The decomposition of the DUS signal using EMD

C. Identification of Cardiac events

After applying EMD to the DUS data, according to the findings in the previous research, the component with the higher frequency band (higher than 100 Hz) i.e. the first IMF, is linked to the valve motions [16]. On the other hand the low frequency components generally correspond to the wall motions.

More precisely, the absolute value of the first IMF has a sequence of peaks which is associated with opening and closure of the atrioventricular and semilunar valves. For a better assessment, the envelope of that IMF was obtained using low-pass filter. The intervals of the cardiac cycles were also found using R-R intervals of the fECG. Then the filtered IMF was normalized over each cardiac cycle and its peaks were detected.

In previous studies, the cardiac events were manually assigned to the peaks and the intervals were calculated. In this paper we aim to identify them automatically. To this end, each peak should be classified as an indicator of one of the cardiac valve timing events or none of them.

The first approach is based on Hidden Markov Model (HMM). It can find the events based on the probabilistic model of their occurrence sequence and timings. However it was also noticed that the amplitude as well as the timing of the peaks can also be used to classify them. Therefore in the next approach, Support Vector Machine (SVM) was used as a powerful classifier to identify the events. Because the temporal dependency of the occurrence of events is not considered in SVM, some extra peaks might be classified as the same event in some cardiac cycles, or a wrong order of events might be noticed. Thus as the last approach Hybrid HMM-SVM is proposed to be used in order to overcome the defects of SVM and HMM. The time segment of each cardiac cycle was set by using fECG as a reference.

1) Hidden Markov Model (HMM): HMM was developed in the 1960s [32] and has been widely used in many signal processing applications. In contrast to the Markov Model, in

This article has been accepted for publication in a future issue of this journal, but has not been fully edited. Content may change prior to final publication. Citation information: DOI 10.1109/JBHI.2013.2286155, IEEE Journal of Biomedical and Health Informatics

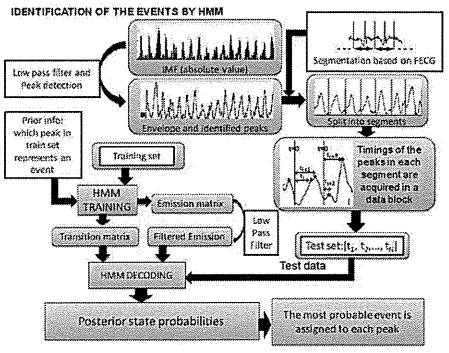

Fig. 3. HMM approach block diagram

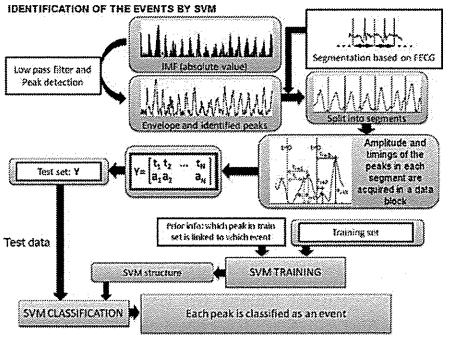

Fig. 4. SVM approach block diagram

HMM the observed symbols are emitted from some hidden states. The formal definition of HMM is [33]:

$$\lambda = (A, B, \pi) \tag{1}$$

A is a transition matrix, B is the emission matrix and π is the initial probability. Given a sequence of observations, the HMM process is aimed to find the sequence of the hidden states that the model went through, based on the transition probability that each state follows another one and the emission probability of the observations from each state. More details can be found in [33]. If there is an available set of examples from a process, the model can be estimated by either supervised or unsupervised training. In this study the supervised approach was used because both input and output of the process were available as a limited training set, for which we had prior information. In our experiments Hidden Markov Models from statistics toolbox of MATLAB was used. In the first approach, HMM was applied to the filtered version of the first IMF for recognizing valve movements. The sample procedure for detecting a cardiac event is shown in figure 3. First the peaks of the first IMF were identified based on the positive first derivative and negative second derivative criteria. In order to find the timing of the peaks of the IMF envelope in each cardiac cycle, the whole sequence had to be split into different segments using the R-R intervals of the fECG. The time difference from the beginning of the segment to the occurrence of each peak in that segment was then calculated, assigned to each peak and denoted by t_i. This data set made our observation set. The hidden states $S = (s_1, s_2, ..., s_N)$ were set as the opening (o) and closure (c) of the Mitral (M) and Aortic (A) valves: Mo, Mc, Ao, Ac and four transitional states: T1, T2, T3, T4, which may occur between each pair of valve motion states.

A training set for which we had prior information about the timings of cardiac events was then used for the HMM training process. First, HMM was trained based on the prior information about the training set (if each peak represented one of the valve motion or transitional events) to provide an estimation of the transition and emission matrices. Each element ij of the transition matrix was estimated as the number of times the event s_j followed s_i in the training set, divided by the total number of s_i in that set. Each element $b_j(k)$ of the emission matrix was estimated by the number of times an observation (peak timing) was linked with the state s_j in the training set, divided by the total number of s_j. Since the training set may not be rich enough to estimate the emission probability for every time bin, the estimated emission matrix may contain many zeros and isolated spikes. Therefore the estimated emission matrix was filtered by a low pass filter and then normalized. This filtered matrix and the transition matrix were then used for HMM, to decode the new data. After decoding, a matrix containing the probability of the occurrence of each event was obtained for each peak. Then the event with the highest estimated probability of occurrence among all events was assigned to each peak.

2) Support Vector Machine (SVM): In this approach, SVM was used to classify the peaks of the IMF envelope as a sign of each event (or no event). SVMs developed by Vapnik [34] are a powerful technique for classification. Two class SVM is designed to find a separating hyperplane with the maximum margin with the classes. In the case of nonlinear classification, the data is first transformed by a Kernel function into the higher dimensional space in which it becomes linearly separable. SVM is based on the "structural risk minimization" criteria in order to attain low probability of generalization error [35]. More details on SVM can be found in [36].

To construct SVMs, a kernel function $K(\mathbf{x}_i, \mathbf{x})$ must be first selected. The choice of the kernel may affect the performance of SVM. The Radial Basis Function (RBF) is one of the kernels which is used in many applications. It is defined as follows:

$$K(\mathbf{x}_i, \mathbf{x}_j) = exp(-\frac{||\mathbf{x}_i - \mathbf{x}_j||^2}{2\sigma^2}) \tag{2}$$

where σ is the width of the RBF function. In this study, the RBF kernel was used and σ was experimentally chosen to be 1.

SVMs are usually formulated for binary (two-class)problems. However they may be extended to multiclass problems. In this study the one-against-all approach was used for multiclass SVM [36]. The classes were the the same as the states in HMM approach.

SVM was used as the second approach for classifying the peaks corresponding to one of the valve motion or other transitional events. For example, the procedure for recognizing an event from the first IMF is shown in figure 4. In order to obtain the features, first EMD was applied to the DUS

This article has been accepted for publication in a future issue of this journal, but has not been fully edited. Content may change prior to final publication. Citation information: DOI 10.1109/JBHI.2013.2286155, IEEE Journal of Biomedical and Health Informatics

data, the envelope of the IMF was taken and all peaks were determined based on the positive first derivative and negative second derivative criteria. Then, the signal was broken into the segments using R-R intervals of FECG as the reference. The time interval from the beginning of each segment to the occurring time of each peak in that segment and the amplitude of the peak were acquired as the features in a matrix **Y**. SVM uses a training set with the prior knowledge which assumes the events associated with the peaks. The SVM structure was developed based on the training set. The new data were classified by SVM to find the event represented by each peak, based on the amplitude and timing of the peaks. The Support Vector Machine functions from Bioinformatics toolbox of MATLAB were used for this study.

3) Hybrid SVM/HMM: The Hybrid SVM/HMM method has been developed for the speech recognition [29], [30]. In this paper we propose to use it for recognizing the cardiac events. It is a combination of HMM and SVM. In order to combine SVM and HMM, a probabilistic output of SVM must be obtained, because HMM is based on probability models. Platt's SVM method [37] can provide such an output. In this method the distance of each sample from the separating hyperplane is transformed to the posterior probability of classifying the sample. The posterior probability output of the SVM, $P(class|input)$, is obtained by calculating: $P(y = +1|f(x))$, where:

$$f(x) = \sum_{i=1}^{l} \alpha_i y_i K(x, x_i) + b \tag{3}$$

and parametric Sigmoid is fitted to the output of the SVM classifier:

$$P(y = +1|f(x)) = \frac{1}{1 + exp(Af(\mathbf{x}) + B)} \tag{4}$$

The parameters A and B are determined by minimizing the negative log likelihood of the training data which has the form of a cross-entropy error function. In the hybrid SVM/HMM process the transition matrix and the initial probability is first determined based on the HMM training process. The SVM is also trained using the training set. The SVM classification process is then performed on the new data and the emission probability distribution is obtained by using the output of the platt's SVM through the Bayes' rule. Therefore the HMM model is constructed. Based on this model, the most probable hidden states are recognized through the decoding process.

For example the procedure of identifying the events from first IMF is shown in figure 5. First the data were broken into segments. Here again, the fECG was used as a reference for segmentation. Then the time and the amplitude of the peaks were taken into the matrix **Y**. A training set for which we had prior information was used for SVM and HMM training. The new data were then classified by the hybrid SVM/HMM method to obtain the probability of the occurrence of the events for each peak. Then one of the valve motion or transitional events for which the estimated occurrence probability was higher than other events was assigned to each peak.

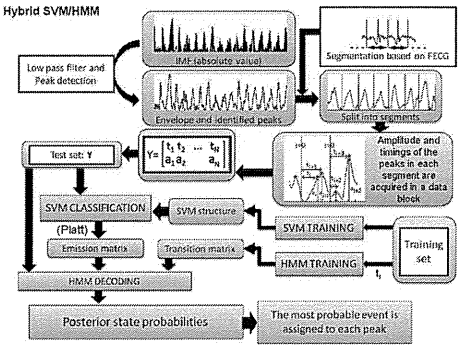

Fig. 5. Hybrid SVM-HMM approach block diagram

TABLE I
MEAN ± STANDARD ERROR OF THE AVERAGE TIME INTERVALS (MSEC) OVER 45 NORMAL FETUSES AND THE ACCURACY OF IDENTIFIED EVENTS.

intervals	Mean± Standard Error	rate (new method)	rate (previous study [17])
R-R	413.6 ± 26.0	100.0%	100.0%
R-Mc	14.3 ± 2.3	91.1%	84.0%
R-Ao	51.1 ± 3.4	95.3%	87.0%
R-Ac	204.6 ± 5.5	98.8%	97.6%
R-Mo	276.4 ± 5.4	94.5%	89.7%
Ao-Ac	153.5 ± 6.3	94.6%	87%

III. RESULTS

In order to evaluate the results, the timings of opening and closure of the valves were verified by the Pulsed-wave Doppler images. It visualizes the direction and the characteristics of the blood flow through the valves. In this technique, the aortic blood flow Doppler waveform is recorded from the long axis of the five-chamber view of the heart. The M-mode cursor is placed perpendicular to the inter-ventricular septum at the level of the mitral valve to examine end-systole and end-diastole (closure of atrioventricular valves).

In this paper the total number of 45 different data sets of DUS and corresponding fECG were used for testing the algorithm and obtaining the timings. In order to train the hybrid SVM/HMM classifier, the timings of the events for 30 cardiac cycles from three different normal fetuses were determined manually based on expertise. The algorithm was then applied to new data sets from different fetuses to find the timings during 40 cardiac cycles for each data set.Figure 6 shows an example of the high frequency IMF and the identified events, the fECG and the Pulsed Doppler image of the mitral valve movement for three cardiac cycles from one of the test sets. Figure 7 shows the result of using another data set with the fECG and the Pulsed Doppler image of the aortic valve movement. Figure 8 shows estimated timings of the valve movements from one of the test data sets. Only few event timings were missed using this method. Table I shows the percentage of the estimated events using all data sets from 45 fetuses and the mean and standard error of the average estimated time intervals over all fetuses.

The identification of the events by using the SVM, HMM and the hybrid SVM/HMM method were compared in

This article has been accepted for publication in a future issue of this journal, but has not been fully edited. Content may change prior to final publication. Citation information: DOI 10.1109/JBHI.2013.2286155, IEEE Journal of Biomedical and Health Informatics

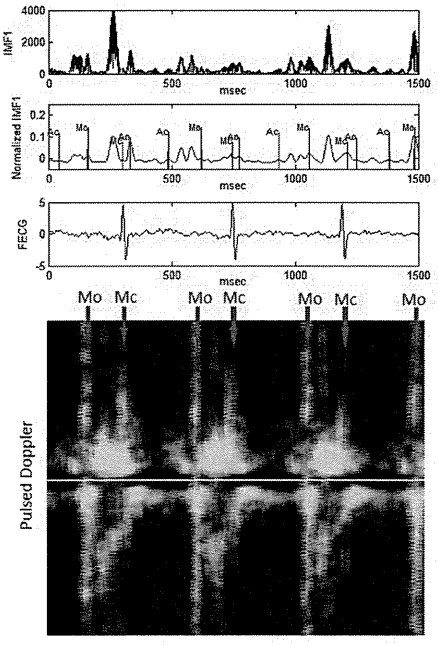

Fig. 6. (a) Shows the first IMF of the Doppler ultrasound signal decomposed by EMD. (b) Shows the envelope of the normalized IMF and the identified timings. (c) Shows an example of the simultaneous fetal electrocardiogram signals extracted from abdominal ECG signals using BSSR. (d) Shows the example of Pulsed wave Doppler signals of fetal mitral valve movements annotated to show how the specific signals are linked with opening and closing events. Mo and Mc represent the opening and closing of mitral valve.

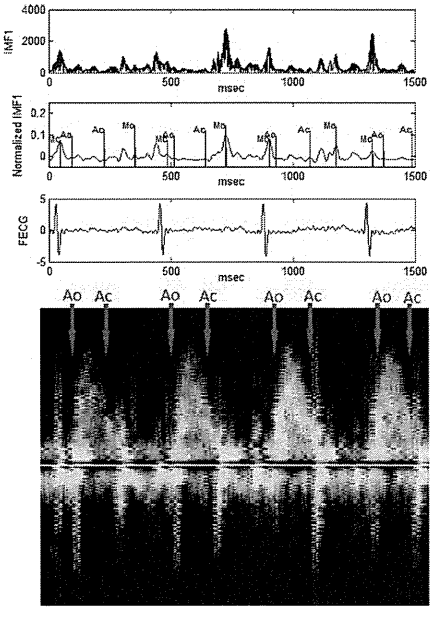

Fig. 7. (a) Shows the first IMF of the Doppler ultrasound signal decomposed by EMD. (b) Shows the envelope of the normalized IMF and the identified timings. (c) Shows an example of the simultaneous fetal electrocardiogram signals extracted from abdominal ECG signals using BSSR. (d) Shows the example of Pulsedwave Doppler signals of fetal Aortic valve movements annotated to show how the specific signals are linked with opening and closing events. Ao and Ac represent the opening and closing of aortic valve.

Figure 9. By comparing the results with the Pulsed Doppler image, it is shown that the hybrid method performs better than our previous study [17].

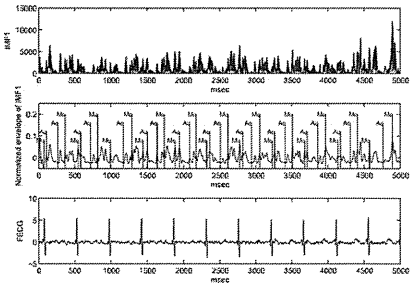

Fig. 8. An example of identified events: mitral opening and closing (Mo and Mc) and aortic valve opening and closing (Ao and Ac).

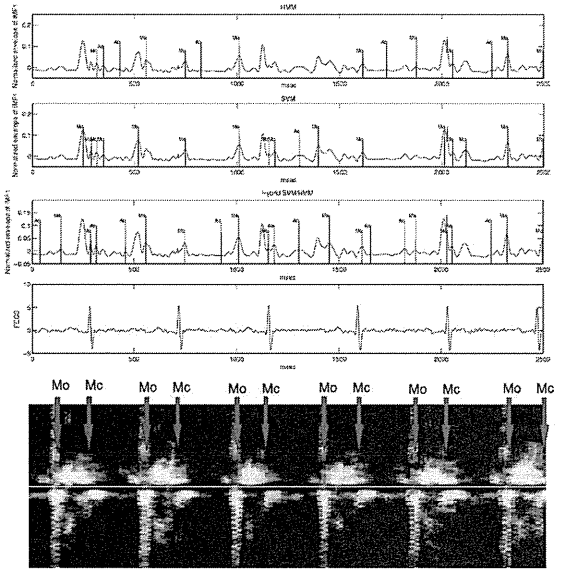

Fig. 9. Comparison of the identification of the valve movements by using HMM (a), SVM (b) and Hybrid SVM/HMM (c)

TABLE II

RESULTS OF KRUSKAL-WALLIS TEST (P-VALUES) AND PAIRWISE COMPARISON WITH MANN-WHITNEY-WILCOXON METHOD FOR CHANGES OF THE ESTIMATED INTERVALS VERSUS DIFFERENT AGE GROUPS. THE MEAN ± STANDARD ERROR (SE) (MSEC) OF THE TIMINGS FOR DIFFERENT AGE GROUPS ARE SHOWN. SIGNIFICANT DIFFERENCES BETWEEN PAIRS OF AGE GROUPS: 16-29 VS 30-35, 16-29 VS 36-41 AND 30-35 VS 36-41 ARE MARKED BY (A), (B) AND (C), RESPECTIVELY.

Interval	p-value	Mean±SE age group 16-29	Mean±SE age group 30-35	Mean±SE age group 36-41
EDT	0.0967	25.3±4.8	24.2±5.5	26.4±4.0
ICT	0.0558	36.4±2.6	35.6±2.7	37.7±3.4
IRT	0.0218	73.0±4.6 (*A*)	69.7±4.5 (*A,C*)	72.2±4.9 (*C*)
PEP	0.0026	61.7±4.8 (*A*)	59.9±5.2 (*A,C*)	64.0±4.0 (*C*)
STI	1×10^{-8}	213.9±5.2 (*B*)	214.0±7.1 (*C*)	218.2±7.1 (*B,C*)
VET	0.0333	152.2±3.7 (*A,B*)	154.2±6.9 (*A*)	154.2±7.7 (*B*)

The estimated intervals were also analyzed by Kruskal-Wallis test to investigate their changes during pregnancy. Data from all 45 fetuses were divided into three different age groups: 16-29, 30-35 and 36-41 weeks, including 15, 12 and 18 fetuses,

This article has been accepted for publication in a future issue of this journal, but has not been fully edited. Content may change prior to final publication. Citation information: DOI 10.1109/JBHI.2013.2286155, IEEE Journal of Biomedical and Health Informatics

TABLE III
RESULTS OF MULTIPLE COMPARISON BY MANN-WHITNEY-WILCOXON METHOD (P-VALUES).

intervals	16-29 vs 30-35	16-29 vs 36-41	30-35 vs 36-41
IRT	0.0032	0.1973	0.0222
PEP	0.0095	0.0966	0.0004
STI	0.4588	0.0000	0.0000
VET	0.0192	0.0091	0.4808

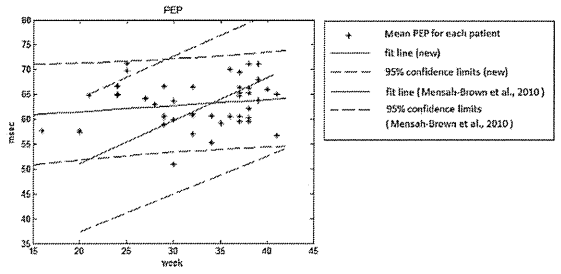

Fig. 10. Changes of the mean and 95% confidence interval of PEP compared to the results of the previous study [38].

respectively. Table II and III show the results of Kruskal-Wallis test (p-values), mean and standard error of the timings for each age group as well as their pair-wise comparison with Mann-Whitney-Wilcoxon method.
Figure 10 shows the result of comparison of the changes in PEP with the findings of an earlier study [38].

IV. DISCUSSION

In previous studies, intervals of cardiac events have been estimated from DUS signal by using digital filtering, STFT or wavelet [8], [16], [17], [20], [39]. The DUS signal is nonlinear and nonstationary and wide changes in the signal content and spectral characteristics are noticed on a beat-to-beat basis. The transient nature of the DUS signal and its variability is also shown in previous papers [16]. Therefore it is not convincing to use fixed parameters such as cut off frequency for filtering methods or wavelet parameters for the whole signal and different subjects. Thus EMD which is a data driven method is more suitable for this application. EMD has been extensively used for decomposing nonlinear and non-stationary signals, including the DUS signal but for estimating the fetal heart rate [27], [28] and it has not been used for this specific application before. The results show that by applying EMD the component which is linked to valve movements is practically separated and its peaks which correspond to the events can be discriminated.
All previous studies were based on manual identification of the cardiac event timings. However it is sometimes difficult to recognize the peaks manually, especially for nonexperts. Moreover the appearance of particular types of events in DUS signal strongly depends on the location of the ultrasound transducer and the fetus. Some peaks which are linked to the cardiac events may not be visible in some situations or some extra peaks may appear which may be confusing for manual recognition. It also takes time to carefully investigate the DUS signal component in order to recognize the events. There are some visual errors as well as inter- and intra- observer errors when events are recognized based on human observation. Therefore in this paper an automated method is proposed to recognize the events. For this purpose the hybrid SVM/HMM method is proposed to be used, which has been previously employed only in speech processing applications. Furthermore, to our best knowledge, the combination of EMD and the hybrid SVM/HMM has never been used before. The hybrid method classifies the peaks of the decomposed component of the DUS signal to be linked to each cardiac event, based on the pattern of the peaks, the timings and the sequence of the events. The better training of the classifier with the DUS signals with different patterns, the more powerful automated recognition of the cardiac events. As shown in table I, by using this method, a higher percentage of the valve movement events was identified, compared to the previous manual method. The results were also compared with the Pulsed Doppler images which verified the successful identification of the events.
The estimation of the timing of cardiac events would have been very difficult without using FECG as a reference for segmentation. In this study the position of the R-waves was used for segmentation of the signal into different cardiac cycles.
Results of this method provide the continuous and beat-to-beat identification of cardiac intervals, which can be used for clinical purposes.
The relationship between the cardiac intervals and the gestational age was also investigated in this study. According to the Kruskal-Wallis test and pairwise comparison with Mann-Whitney-Wilcoxon, STI was found to be the most changeable with the age. On the other hand ICT was more stable during pregnancy as also reported by Koga [15]. According to a recent study by Mensah-Brown et al., PEP increases with the gestational age (r= 0.57 , $p < 0.0001$) [38]. In this study based on the pairwise comparison, it is found that PEP slightly decreases ($p < 0.0095$) from the age group of 16-29 to 30-35, and then significantly increases to the age of 36-41 ($p = 0.0004$, table III). As shown in figure 10 the estimated timings are mostly in the same range of 95% confidence interval of the previous study [38], especially after 30 weeks. The results of pairwise comparison indicate that except for EDT and ICT, all intervals of the age group 36-41 are significantly different from previous ages. For example STI does not change significantly from the age of 16-29 to 30-35 ($p = 0.4588$), but after that sharply increases toward the final weeks of pregnancy ($p < 0.0001$). The trend of changes in PEP is also different in the final stage. Therefore the final weeks of pregnancy are the most critical.
IRT intervals were found to be longer in this study than the timings reported in [40]. The reason may be that the age of the fetuses analyzed in [40] was from 6 to 10 weeks of gestation, but the average age of the fetuses we analysed was 31 weeks. The cardiac function changes with the development of the fetal heart. A part of the difference may be related to this developmental change.
A limitation of this study is that the quantitative comparison with the pulsed wave Doppler image based valve motion timings were not provided. More accurate methods such as

This article has been accepted for publication in a future issue of this journal, but has not been fully edited. Content may change prior to final publication. Citation information: DOI 10.1109/JBHI.2013.2286155, IEEE Journal of Biomedical and Health Informatics

trans-vaginal pulsed Doppler imaging can be used in the first trimester foetuses [40]. However our system is compatible with this wide-continuous monitoring of fetal heart during second to third trimesters. More accurate quantitative comparison of the results of the proposed method with pulsed Doppler images requires image processing and recognition process which is beyond the scope of this study. The quantitative comparison can be done in future studies.

V. Conclusion

DUS signal is nonlinear, non stationary, noisy and it is variable on a beat to beat basis. Therefore using a combination of EMD as a data driven method for decomposing nonlinear and nonstationary signal and hybrid SVM/HMM for automated identification of the events improves the estimation of cardiac intervals. Results show that 94.5% of mitral opening, 91.1% of mitral closing, 95.3% of aortic valve opening and 98.8% of aortic valve closing were identified by this method, which were higher than the manual approaches. The identified timings were verified by pulsed doppler images.

Furthermore the trend of changes of the cardiac intervals for growing gestational age groups was analysed. Results show that STI, IRT, VET and PEP change significantly from early to late gestational fetuses. In particular the intervals which correspond to the last weeks before delivery are significantly different from their values during the earlier weeks.

Acknowledgment

This study was supported by an Australian Research Council Linkage grant (LP100200184) with Tohoku University and Atom Medical Corporation in Japan. The authors would like to thank a team of clinical support service at Tohoku University in Japan for fetal Doppler data recording and fetal ECG extraction from abdominal ECG data.

References

[1] "Congenital heart defects in children fact sheet,"

[2] J. Hoffman, "Incidence of congenital heart disease: Ii. prenatal incidence," *Pediatric cardiology*, vol. 16, no. 4, pp. 155–165, 1995.

[3] E. Merz, *Ultrasound in Obstetrics and Gynecology*. Georg Thieme Verlag, 2004.

[4] A. B. Hameed and M. S. Sklansky, "Pregnancy: maternal and fetal heart disease," *Current problems in cardiology*, vol. 32, no. 8, pp. 419–494, 2007.

[5] P. Malcus, "Antenatal fetal surveillance," *Current Opinion in Obstetrics and Gynecology*, vol. 16, no. 2, pp. 123–128, 2004.

[6] R. P. Lewis, S. Rittogers, W. Froester, and H. Boudoulas, "A critical review of the systolic time intervals.," *Circulation*, vol. 56, no. 2, pp. 146–158, 1977.

[7] A. M. Weissler, W. S. Harris, and C. D. Schoenfeld, "Systolic time intervals in heart failure in man," *Circulation*, vol. 37, no. 2, pp. 149–159, 1968.

[8] Y. MURATA and J. CHESTER B MARTIN, "Systolic time intervals of the fetal cardiac cycle," *Obstetrics & Gynecology*, vol. 44, no. 2, pp. 224–232, 1974.

[9] Y. Yumoto, S. Satoh, Y. Fujita, T. Koga, N. Kinukawa, and H. Nakano, "Noninvasive measurement of isovolumetric contraction time during hypoxemia and acidemia: Fetal lamb validation as an index of cardiac contractility," *Early human development*, vol. 81, no. 7, pp. 635–642, 2005.

[10] I. E. ZADOR, R. N. WOLFSON, S. K. PILLAY, I. E. TIMOR-TRITSCH, and R. H. HERTZ, "Fetal cardiac time intervals and their potential clinical applications," *Clinical Obstetrics and Gynecology*, vol. 22, no. 3, pp. 651–663, 1979.

[11] L. Caserta, Z. Ruggeri, L. D'Emidio, C. Coco, P. Cignini, A. Girgenti, L. Mangiafico, and C. Giorlandino, "Two-dimensional fetal echocardiography: where we are," *Journal of prenatal medicine*, vol. 2, no. 3, p. 31, 2008.

[12] Y. Murata, C. B. Martin, T. Ikenoue, and P. Lu, "Antepartum evaluation of the pre-ejection period of the fetal cardiac cycle," *Am J Obstet Gynecol*, vol. 132, pp. 278–284, 1978.

[13] L. Organ, A. Bernstein, and P. Hawrylyshyn, "The pre-ejection period as an antepartum indicator of fetal well-being.," *American journal of obstetrics and gynecology*, vol. 137, no. 7, p. 810, 1980.

[14] M. B. SAMPSON, "Antepartum measurement of the preejection period in high-risk pregnancy," *Obstetrics & Gynecology*, vol. 56, no. 3, pp. 289–290, 1980.

[15] T. Koga, N. Athayde, and B. Trudinger, "The fetal cardiac isovolumetric contraction time in normal pregnancy and in pregnancy with placental vascular disease: the first clinical report using a new ultrasound technique," *British Journal of Obstetrics and Gynaecology*, vol. 108, no. 2, pp. 179–185, 2001.

[16] S. Shakespeare, J. Crowe, B. Hayes-Gill, K. Bhogal, and D. James, "The information content of doppler ultrasound signals from the fetal heart," *Medical and Biological Engineering and Computing*, vol. 39, no. 6, pp. 619–626, 2001.

[17] A. H. Khandoker, Y. Kimura, T. Ito, N. Sato, K. Okamura, and M. Palaniswami, "Antepartum non-invasive evaluation of opening and closing timings of the cardiac valves in fetal cardiac cycle," *Medical & biological engineering & computing*, vol. 47, no. 10, pp. 1075–1082, 2009.

[18] M. Sato, Y. Kimura, S. Chida, T. Ito, N. Katayama, K. Okamura, and M. Nakao, "A novel extraction method of fetal electrocardiogram from the composite abdominal signal," *Biomedical Engineering, IEEE Transactions on*, vol. 54, no. 1, pp. 49–58, 2007.

[19] A. Khandoker, Y. Kimura, and M. Palaniswami, "Automated identification of abnormal fetuses using fetal ecg and doppler ultrasound signals," in *Computers in Cardiology, 2009*, pp. 709–712, IEEE, 2009.

[20] A. H. Khandoker, Y. Kimura, M. Palaniswami, and S. Marusic, "Identifying fetal heart anomalies using fetal ecg and doppler cardiogram signals," in *Computing in Cardiology, 2010*, pp. 891–894, IEEE, 2010.

[21] N. E. Huang, Z. Shen, S. R. Long, M. C. Wu, H. H. Shih, Q. Zheng, N.-C. Yen, C. C. Tung, and H. H. Liu, "The empirical mode decomposition and the hilbert spectrum for nonlinear and non-stationary time series analysis," *Proceedings of the Royal Society of London. Series A: Mathematical, Physical and Engineering Sciences*, vol. 454, no. 1971, pp. 903–995, 1998.

[22] B. Mijovic, M. De Vos, I. Gligorijevic, J. Taelman, and S. Van Huffel, "Source separation from single-channel recordings by combining empirical-mode decomposition and independent component analysis," *Biomedical Engineering, IEEE Transactions on*, vol. 57, no. 9, pp. 2188–2196, 2010.

[23] J. C. Nunes, Y. Bouaoune, E. Delechelle, O. Niang, and P. Bunel, "Image analysis by bidimensional empirical mode decomposition," *Image and vision computing*, vol. 21, no. 12, pp. 1019–1026, 2003.

[24] A. Bouzid and N. Ellouze, "Empirical mode decomposition of voiced speech signal," in *Control, Communications and Signal Processing, 2004. First International Symposium on*, pp. 603–606, IEEE, 2004.

[25] C. M. Sweeney-Reed and S. J. Nasuto, "A novel approach to the detection of synchronisation in eeg based on empirical mode decomposition," *Journal of Computational Neuroscience*, vol. 23, no. 1, pp. 79–111, 2007.

[26] J. Echeverria, J. Crowe, M. Woolfson, and B. Hayes-Gill, "Application of empirical mode decomposition to heart rate variability analysis," *Medical and Biological Engineering and Computing*, vol. 39, no. 4, pp. 471–479, 2001.

[27] B. Krupa, M. M. Ali, and E. Zahedi, "The application of empirical mode decomposition for the enhancement of cardiotocograph signals," *Physiological measurement*, vol. 30, no. 8, p. 729, 2009.

[28] D. Rouvre, D. Kouamé, F. Tranquart, and L. Pourcelot, "Empirical mode decomposition (emd) for multi-gate, multi-transducer ultrasound doppler fetal heart monitoring," in *Signal Processing and Information Technology, 2005. Proceedings of the Fifth IEEE International Symposium on*, pp. 208–212, IEEE, 2005.

[29] A. Ganapathiraju, J. Hamaker, and J. Picone, "Hybrid svm/hmm architectures for speech recognition.," in *INTERSPEECH*, pp. 504–507, Citeseer, 2000.

[30] M. Gurban and J.-P. Thiran, "Audio-visual speech recognition with a hybrid svm-hmm system," in *13th European Signal Processing Conference*, 2005.

This article has been accepted for publication in a future issue of this journal, but has not been fully edited. Content may change prior to final publication. Citation information: DOI 10.1109/JBHI.2013.2286155, IEEE Journal of Biomedical and Health Informatics

[31] E. Symonds, D. Sahota, and A. Chang, *Fetal Electrocardiology*. London: Imperial College Press, 2001.
[32] L. E. Baum, T. Petrie, G. Soules, and N. Weiss, "A maximization technique occurring in the statistical analysis of probabilistic functions of markov chains," *The annals of mathematical statistics*, vol. 41, no. 1, pp. 164–171, 1970.
[33] P. Blunsom, "Hidden markov models," *Lecture notes, August*, 2004.
[34] V. Vapnik, *The nature of statistical learning theory*. springer, 2000.
[35] S. Haykin, *Neural networks: a comprehensive foundation*. Prentice Hall PTR, 1994.
[36] S. Abe, *Support vector machines for pattern classification*. Springer, 2010.
[37] J. Platt *et al.*, "Probabilistic outputs for support vector machines and comparisons to regularized likelihood methods," *Advances in large margin classifiers*, vol. 10, no. 3, pp. 61–74, 1999.
[38] N. A. Mensah-Brown, R. T. Wakai, B. Cheulkar, S. Srinivasan, and J. F. Strasburger, "Assessment of left ventricular pre-ejection period in the fetus using simultaneous magnetocardiography and echocardiography," *Fetal diagnosis and therapy*, vol. 28, no. 3, pp. 167–174, 2010.
[39] T. Kupka, J. Jezewski, A. Matonia, K. Horoba, and J. Wrobel, "Timing events in doppler ultrasound signal of fetal heart activity," in *Engineering in Medicine and Biology Society, 2004. IEMBS'04. 26th Annual International Conference of the IEEE*, vol. 1, pp. 337–340, IEEE, 2004.
[40] K. Mäkikallio, P. Jouppila, and J. Räsänen, "Human fetal cardiac function during the first trimester of pregnancy," *Heart*, vol. 91, no. 3, pp. 334–338, 2005.

Faezeh Marzbanrad received the B.Sc. and M.Sc. degrees in electrical engineering from Shiraz University, Shiraz, Iran, in 2007 and 2010 respectively. She is currently a Ph.D. student in the department of electrical and electronic engineering, the University of Melbourne, Parkville, Australia. Her research interests include statistical signal processing, time-frequency analysis and machine learning, with special emphasis on fetal cardiac assessment.

Yoshitaka Kimura received the Master of Science degree in mathematics in 1982 and the M.D. degree in 1997 from Tohoku University, Sendai, Japan. From 1998 to 2004, he was a Lecturer in the Departments of Obstetrics and Gynecology, Tohoku University Graduate school of Medicine. From 2003 to 2004, he was a Visiting Researcher at New York University Medical Center. From 2004 to 2012, he was a Professor in the Telecommunication and Information Technology of Tohoku University Biomedical Engineering Research Organization. Since 2012, he has been a Professor in the Graduate School of Medicine, Disability Science, Advanced Interdisciplinary Biomedical Engineering, Tohoku University, and Graduate School of Biomedical Engineering, Next Generation Biological Information Technology, Tohoku University. His research focuses on detection, processing, and interpretation of fetal electrocardiogram for the clinical diagnosis and his interest's concern combination of the information theory with the infinite dimensional geometry to analyze the nonlinear and non-stationary signals.

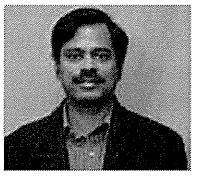

Marimuthu Palaniswami (S84M87SM94F12) received the M.E. degree from the Indian Institute of Science, Bangalore, India, the M.Eng.Sc. degree from The University of Melbourne, Parkville, Australia, and the Ph.D. degree from the University of Newcastle, Callaghan, Australia. He is currently a Professor with the Department of Electrical and Electronic Engineering, The University of Melbourne. He has published over 400 refereed research papers and leads one of the largest funded Australian Research Council, Research Network on Intelligent Sensors, Sensor Networks, and Information Processing programme. He has been a grants panel member for NSF, an advisory board member for the European FP6 grant center, a steering committee member for National Collaborative Research Infrastructure Strategy, Great Barrier Reef Ocean Observing System, Smart Environmental Monitoring and Analysis Technologies, and a board member for Information Technology and supervisory control and data acquisition companies. He has been funded by several ARC and industry grants (over 40 m) to conduct research in sensor network, Internet of things (IoT), health, environmental, machine learning, and control areas. He is representing Australia as a core partner in European Union FP7 projects such as SENSEI, SmartSantander, Internet of Things Initiative, and SocIoTal. His research interests include support vector machines sensors and sensor networks, IoT, machine learning, neural network, pattern recognition, signal processing, and control.

Ahsan Khandoker (M07SM12) received the B.Sc. Electrical and Electronic Engineering from Bangladesh University of Engineering and Technology (BUET).Dhaka, Bangladesh in 1996, M. EngSc in 1999 from Multimedia University (MMU), Malaysia and M. Engg in 2001 and Doctor of Engineering in physiological engineering from Muroran Institute of Technology (MIT), Japan in 2004. He is currently working as an Assistant Professor in the department of Biomedical Engineering at Khalifa University in Abu Dhabi, UAE. He is also working as Senior Research Fellow for Australian Research Council Research Networks on Intelligent Sensors, Sensor Networks and Information Processing (ISSNIP) at the University of Melbourne in Australia. He has published 35 peer-reviewed journal articles and over 75 conference papers the research field of physiological signal processing and modeling in fetal cardiac disorders, sleep disordered breathing, diabetic autonomic neuropathy, and human gait dysfunction, and is passionate about research helping clinicians to noninvasively diagnose diseases at early stage. He has also worked with several Australian Medical device manufacturing industries, as well as hospitals as a research consultant focusing on integration of technology in clinical settings.

J Neurosurg Pediatrics 10:7–13, 2012

Complete remission of seizures after corpus callosotomy

Clinical article

Masaki Iwasaki, M.D.,[1] Mitsugu Uematsu, M.D.,[2] Yuko Sato, M.D.,[2] Tojo Nakayama, M.D.,[2] Kazuhiro Haginoya, M.D.,[3] Shin-ichiro Osawa, M.D.,[1] Hisashi Itabashi, M.D.,[4] Kazutaka Jin, M.D.,[4] Nobukazu Nakasato, M.D.,[4] and Teiji Tominaga, M.D.[1]

Departments of [1]Neurosurgery, [2]Pediatrics, and [4]Epileptology, Tohoku University Graduate School of Medicine; and [3]Division of Pediatric Neurology, Takuto Rehabilitation Center for Children, Sendai, Japan

Object. Corpus callosotomy is usually intended to alleviate—not to achieve total control of—epileptic seizures. A few patients experience complete seizure control after callosotomy, but the associated clinical factors are unknown. The object of this study was to investigate clinical factors associated with long-term seizure remission after total corpus callosotomy in patients with infantile or early childhood onset epilepsy.

Methods. Thirteen consecutive patients with infantile or early childhood onset epilepsy underwent 1-stage total corpus callosotomy for alleviation of seizures. Their age at surgery ranged from 1 year and 5 months to 24 years (median 7 years). Eleven patients had West syndrome at the onset of disease, and the other 2 had Lennox-Gastaut syndrome. All patients suffered from spasms, axial tonic seizures, or atonic seizures. Six patients had proven etiology of epilepsy, including tuberous sclerosis, polymicrogyria, trauma, and Smith-Magenis syndrome. The association between postoperative seizure freedom and preoperative factors including age at surgery, no MRI abnormalities, proven etiology, and focal electroencephalographic epileptiform discharges was examined.

Results. Postoperative seizure freedom was achieved in 4 of 13 patients for a minimum of 12 months. All 4 patients had no MRI abnormalities and no identified etiology. None of the 8 patients with MRI abnormality, 6 patients with known etiology of epilepsy, or 4 patients aged older than 10 years at surgery achieved seizure freedom. Two of the 7 patients with focal electroencephalographic abnormalities became seizure free. Absence of MRI abnormalities was significantly associated with postoperative seizure freedom ($p < 0.01$).

Conclusions. Complete seizure remission is achieved after total corpus callosotomy in a subgroup of patients with intractable epilepsy following West syndrome or Lennox-Gastaut syndrome. One-stage total corpus callosotomy at a young age may provide a higher rate of seizure freedom, especially for patients with no MRI abnormalities and no identified etiology of epilepsy.
(http://thejns.org/doi/abs/10.3171/2012.3.PEDS11544)

Key Words • **epilepsy surgery** • **West syndrome** • **corpus callosotomy** • **seizure outcome** • **pediatric epilepsy**

Corpus callosotomy has been established as a palliative treatment for patients with intractable epilepsy who are not candidates for resective surgery.[5,8,9,14,19] Long-term postoperative outcomes have demonstrated the safety and effectiveness of the procedure.[2,16–18] Meaningful (50% or greater) seizure reduction is seen in more than 70% of patients. Corpus callosotomy is especially effective for suppressing drop attacks and generalized tonic-clonic seizures.[7,16] Corpus callosotomy achieves seizure freedom from drop attacks in more than 80% of patients.[15] Total section of the corpus callosum is more effective than partial section.[4]

Corpus callosotomy is employed as a last resort in most situations, because the indications and efficacy are not definitive. The efficacy of corpus callosotomy has been measured by various criteria, such as more than 50% seizure reduction, more than 75% reduction, or freedom from drop episodes.[2,16,17] Corpus callosotomy results in complete seizure remission in a small number of patients.[2,16] Up to 10% of patients experience Engel Class I outcome after surgery.[2,16,17] However, the clinical factors indicating such curative outcome have never been investigated.

In the present study we retrospectively investigated

Abbreviations used in this paper: ACTH = adrenocorticotropic hormone; AED = antiepileptic drug; DQ = developmental quotient; EEG = electroencephalography.

the clinical factors associated with long-term seizure remission after total corpus callosotomy in patients with infantile or early childhood onset epilepsy.

Methods

This study was approved by the Tohoku University Graduate School of Medicine institutional review board.

Study Population

This study included 13 consecutive patients with infantile or early childhood onset epilepsy who underwent 1-stage total corpus callosotomy for alleviation of seizures. The patients' characteristics are summarized in Table 1. All patients underwent comprehensive evaluation of epilepsy including video-EEG monitoring, 3T MRI, and FDG-PET. Patients were qualified for surgical treatment after a management conference. Their age at epilepsy onset ranged from 11 days to 28 months (median 7 months). Their age at surgery ranged from 1 year 5 months to 24 years (median 7 years).

Eleven patients were diagnosed with West syndrome at the onset of disease. Another 2 patients (Cases 4 and 13) had an electroclinical diagnosis of Lennox-Gastaut syndrome. Magnetic resonance imaging was performed in all cases. Skin examination, metabolic screening, fundoscopy, and chromosomal analysis were also performed as required. In 6 patients a causal condition (tuberous sclerosis, traumatic brain injury, diffuse polymicrogyria, or Smith-Magenis syndrome) was identified. In 7 patients there was no proven etiology; brain MRI showed mild to moderate atrophy in 2 of these 7, and no abnormality in 5. Interictal EEG was characterized by generalized and/or multifocal epileptiform discharges in all patients. No patients had focal or lateralized features as part of the seizure semiology. Twelve of the 13 patients suffered from drop attacks; the 1 patient who did not (Case 12) was largely bedridden due to severe developmental delay. Drop attacks were defined as seizure-related falls causing injury to the body or head, not as a specific seizure type, in this study. Spasms, tonic seizures, or atonic seizures could cause drop attacks. All patients presented with developmental delay or regression at the time of surgery. Ten patients with the initial diagnosis of West syndrome received ACTH therapy in the early course of the disease. Medication with 5 or more AEDs had failed to control seizures in all patients.

Corpus Callosotomy

One-stage total corpus callosotomy was performed with right paramedian frontal craniotomy.[6] The patient was positioned supine with no head rotation. The head was elevated so that the anterior part of the corpus callosum was approached perpendicularly. Sufficient working space was available in all patients anterior to the coronal suture and no bridging veins were sacrificed, although MR venography was routinely performed to evaluate the bridging veins to the superior sagittal sinus. The arachnoid membrane of the interhemispheric fissure was sharply dissected to expose the surface of the corpus callosum between the anterior cerebral arteries. First, the dissection was advanced anteriorly to identify the anterior end of the callosum, where the anterior cerebral arteries course ventrally along the callosal surface. Then, aspiration of the corpus callosum was started approximately 2 cm posterior to that point. Care was taken to maintain gentle aspiration at the midline to open the cavity of the septum pellucidum but not to enter the lateral ventricle. The cavity of the septum pellucidum is typically identified as a narrow space without subependymal vasculature. Once the cavity is opened, sectioning of the corpus callosum was performed as if breaking the "roof" of the cavity over its entire length. Fine subpial aspiration was performed by following the anterior cerebral arteries at the genu and rostrum, and by following the splenial veins at the splenium. The patient's head was lowered when sectioning the splenium, such that the posterior part of corpus callosum was perpendicular to the floor.

Postoperative Follow-Up and Outcome Evaluation

Postoperative MRI was performed at 7 days after surgery. Patients were followed up with continuation of antiepileptic medication by pediatric neurologists. Seizure outcome was evaluated at the outpatient clinic using numbers of total seizures and drop attacks, both measured as reduction of the frequency relative to preoperative state. Seizure freedom was defined as seizures being completely controlled for more than 12 months. The association between postoperative seizure freedom and preoperative factors (including an age of less than 10 years at the time of surgery, normal MRI findings, proven etiology, and presence of focal epileptiform discharges on EEG) was examined with the Fisher exact test.

Results

Seizure Outcome

Postoperative MRI confirmed complete section of the corpus callosum in all patients. The duration of follow-up ranged from 8 to 35 months (median 19 months). Complete seizure remission was achieved postoperatively in 4 patients for a minimum of 12 months. The frequency of seizures was reduced by 50% or greater in 3 other patients and remained unchanged in 6 patients. However, all of these 9 patients experienced appreciable reduction of seizure intensity. In 8 of these patients, spasms or tonic seizures persisted but did not cause drop attacks; in the other patient, drop attacks were reduced by 90%.

Long-term seizure remission was obtained immediately after surgery and was sustained in 3 patients. One patient (Case 1) experienced relapse of epileptic spasms at 10 months after surgery but regained seizure freedom within 1 month after adjustment of medication and remained seizure free for the following 20 months. Of the 9 patients without complete seizure remission, 5 patients (Cases 8–11 and 13) continued to have seizures from the immediate postoperative period. Four patients experienced short-term remission immediately after surgery, but suffered seizure relapse—within 2 weeks in 3 patients, and within 3 months in 1.

The number of AEDs was reduced postoperatively

TABLE 1: Clinical and demographic characteristics of 13 patients who underwent corpus callosotomy*

Case No.	Age (yrs),† Sex	Age (mos) at Ep Onset	Ep Syndrome at Onset	Etiology	MRI	EEG	Seizure Types	Previous Tx	Preop AED	Seizure Outcome‡		AEDs at Last FU	Postop FU (mos)
										All Seizures	Drop Attacks		
1	7, F	6	West	NI	NML	multifocal	spasm, axial tonic, atonic	ACTH, VPA, TPM, ZNS, CLB, loflazepam, KBr	ZNS, TPM, CLB, KBr	free	free	ZNS, TPM, CLB	31
2	6, M	19	West	NI	NML	gen SSWC	spasm, axial tonic	ACTH, VPA, PHT, PB, ZNS, CZP, NZP, loflazepam, KBr, sultiame	VPA, ZNS	free	free	VPA, ZNS	17
3	4, F	7	West	NI	NML	gen & multifocal	axial tonic	ACTH, vit B6, VPA, LTG, TPM, ZNS, CZP, ketogenic diet	VPA, TPM, CZP	free	free	VPA, TPM, CZP	16
4	4, F	28	LGS	NI	NML	gen SSWC	axial tonic	VPA, LTG, TPM, CZP, CLB, NZP	VPA, LTG, CLB	free	free	VPA, LTG	13
5	24, M	3	West	NI	NML	gen SSWC	atonic-tonic, axial tonic-clonic	ACTH, vit B6, VPA, PHT, CBZ, LTG, ZNS, LEV, NZP, ESM	CBZ, LTG, ZNS	no change	free	CBZ, LEV, CLB	19
6	5, M	19	West	NI	general atrophy	gen	spasm	ACTH ×2, vit B6, VPA, PHT, LTG, TPM, ZNS, GBP, CLB, CZP, NZP, acetazolamide	VPA, LTG, CLB	>75% reduction	free	VPA, LTG, CZP	35
7	20, M	7	West	NI	general atrophy	gen & multifocal	axial tonic	ACTH ×3, VPA, PHT, CBZ, PB, LTG, TPM, ZNS, GBP, CZP, CLB, sultiame	VPA, LTG, CLB, sultiame	no change	free	VPA, LTG, sultiame	22
8	6, F	9	West	Smith-Magenis syndrome	general atrophy	gen SSWC & multifocal	spasm, axial tonic	ACTH ×2, VPA, PHT, PB, LTG, TPM, ZNS, ESM, CZP, DZP, CLB	PB, CLB	50% reduction	free	PB, CLB, LEV	19
9	1.4, F	1	West	tuberous sclerosis	multiple tubers	gen & multifocal	axial tonic	ACTH ×2, VPA, PB, ZNS, TPM, CZP	VPA, PB, TPM, CZP	no change	free	CBZ, LEV, ZNS, CLB	25
10	8, F	<1	West	tuberous sclerosis	rt frontal tuber	gen & focal	atonic-tonic	ACTH, VPA, PHT, CBZ, PB, LTG, TPM, CZP, DZP, loflazepam, KBr	VPA, PHT, LTG, loflazepam	no change	>90% reduction	VPA, PHT, loflazepam	21
11	17, F	3	West	tuberous sclerosis	multiple tubers	gen & multifocal	axial tonic, tonic-clonic	ACTH, vit B6, VPA, PHT, CBZ, PB, LTG, ZNS, GBP, CZP, CLB, NZP, loflazepam, KBr, LEV, op	CBZ, LTG, LEV, loflazepam	no change	free	CB, VPA, LTG, CLB	8

(continued)

TABLE 1: Clinical and demographic characteristics of 13 patients who underwent corpus callosotomy* (*continued*)

Case No.	Age (yrs),† Sex	Age (mos) at Ep Onset	Ep Syndrome at Onset	Etiology	MRI	EEG	Seizure Types	Previous Tx	Preop AED	Seizure Outcome‡		AEDs at Last FU	Postop FU (mos)
										All Seizures	Drop Attacks		
12	14, M	4	West	polymicrogyria	bilat polymicrogyria	gen SSWC	axial tonic	VPA, PHT, CBZ, PB, TPM, ZNS, DZP, CLB, NZP, loflazepam, KBr, sultiame, vit B6, acetazolamide	VPA, TPM, loflazepam, acetazolamide	>90% reduction	—	VPA, PB, TPM, loflazepam	10
13	7, M	16	LGS	trauma	lt occipital ulegyria	gen SSWC	spasm, axial tonic, absence	VPA, PHT, PB, LTG, TPM, ZNS, CZP, CLB, ESM	VPA, PB, CLB, ESM	no change	free	VPA, LTG, CLB, ESM	12

* CBZ = carbamazepine; CLB = clobazam; CZP = clonazepam; DZP = diazepam; Ep = epilpesy; ESM = ethosuximide; FU = follow-up; GBP = gabapentin; gen = generalized; KBr = potassium bromide; LEV = levetiracetam; LGS = Lennox-Gastaut syndrome; LTG = lamotrigine; NI = not identified; NML = normal; NZP = nitrazepam; PB = phenobarbital; PHT = phenytoin; SSWC = slow spike wave complexes; TPM = topiramate; Tx = treatment; vit = vitamin; VPA = valproic acid; West = West syndrome; ZNS = zonisamide.

† Age at surgery.

‡ Change in frequency relative to baseline.

in 2 of 4 patients who achieved complete seizure remission, and in the other 2 the number remained the same. Among the 9 patients with postoperative seizures, the number of AEDs was reduced in 3 patients and increased in 1 patient. One patient (Case 9) underwent resective epilepsy surgery 25 months after corpus callosotomy. For purposes of the present study, seizure outcome was evaluated in this case at the last follow-up examination before the second surgery. No other patients received any additional surgical treatment (including vagus nerve stimulation) postoperatively. Interictal epileptiform discharges were present in postoperative electroencephalograms in all patients. Although reduction in their frequency and improvement in the posterior background activities were frequent findings, no clear association with outcome was observed. Electroencephalographic changes after corpus callosotomy have been reported previously.[3]

Preoperative Factors and Outcome

All 4 patients with complete seizure remission had no abnormality in preoperative MRI or any identified etiology. None of the 8 patients with MRI abnormality, 6 patients with known etiology of epilepsy, or 4 patients aged older than 10 years at surgery achieved seizure freedom. Two of the 7 patients with focal electroencephalographic abnormalities became seizure free. Absence of MRI abnormalities was significantly associated with complete seizure remission ($p < 0.01$). No other factors including an age at surgery of less than 10 years, proven etiology, and presence of focal epileptiform discharges in electroencephalograms had any statistical association with seizure remission.

Neurological Outcome

No surgical complications were seen. A slight decrease in spontaneity was transiently seen in 6 patients as a part of the postoperative disconnection syndrome, but it required no medical intervention and resolved within 7 days. No permanent neurological or behavioral deterioration was observed. One patient (Case 2) suffered transient alien hand syndrome in the left extremity for 3 months. Improvements in attention and behavior were usually noted by parents.

Illustrative Case

Case 3

This young girl with intractable epilepsy was referred for surgical treatment of epilepsy at the age of 4 years and 1 month. Her birth and perinatal history were uneventful. She had no family history of epilepsy or seizures. She was developmentally normal at least until age 4 months and started to suffer clusters of epileptic spasms at the age of 7 months. Interictal EEG showed marked hypsarrhythmia, and her DQ was as low as 74. Treatment was started under a diagnosis of West syndrome. Administration of valproate and vitamin B6 failed to control her seizures, so a course of ACTH therapy was initiated at the age of 8 months. She had short-term remission of seizures afterward, but her seizures recurred at the age of 12 months.

Since then, her seizures had been resistant to multiple antiepileptic medications including valproate, lamotrigine, topiramate, zonisamide, and clonazepam. The duration and intensity of the seizures gradually increased with age. She was suffering axial tonic seizures 5–10 times a day at the age of 3 years, which caused frequent episodes of falling and head injury. At age 3 years 7 months, she started to lose the ability to walk because of frequent seizures. At that time, she was taking valproate 240 mg, topiramate 40 mg, and clonazepam 1 mg per day. She was evaluated for surgical treatment of epilepsy.

Twenty-four–hour video-electroencephalographic recording revealed a diffuse decremental pattern with no focal epileptic discharges at the onset of tonic seizures. Interictal EEG was characterized by generalized polyspikes and waves, and occasional left and right frontocentral spikes (Fig. 1). No abnormalities were revealed by 3T brain MRI, including FLAIR, T2-weighted, and 3D magnetization-prepared rapid acquisition gradient echo sequences. Interictal FDG-PET and iomazenil-SPECT showed no focal decrease of uptake. Corpus callosotomy was recommended at the case management conference to reduce the risk of seizure-related injury. The patient's preoperative DQ was 17. She underwent total corpus callosotomy with right paramedian frontal craniotomy (Fig. 2).

The postoperative course was uneventful and the patient did not show signs of disconnection syndrome. Postoperative MRI confirmed complete section of the corpus callosum (Fig. 3). Antiepileptic medications were continued as before surgery. The patient has been completely seizure free for 13 months. Her parents noticed improvement in her hyperactive behavior, and she regained the ability to walk 6 months after surgery. Her DQ at 1 year after surgery was 16.

Discussion

This study shows that complete seizure remission can be achieved after total corpus callosotomy in a subgroup of patients with intractable epilepsy following West syndrome or Lennox-Gastaut syndrome. One-stage total corpus callosotomy at a young age may provide higher rates of seizure freedom, especially for patients with no MRI abnormality and no identified etiology. The present study involved only a small number of patients, but suggested that absence of MRI abnormality was associated with postoperative seizure freedom. No patient with abnormal findings on MRI or proven etiology of epilepsy achieved seizure freedom.

Application of total callosotomy for pediatric patients is a major reason for the high rate of complete seizure remission in our study. Total callosotomy is clearly more effective than partial or anterior callosotomy in seizure reduction.[4,15] A high rate of complete seizure remission was observed in a study that primarily employed total callosotomy,[16] and 1-stage total callosotomy is increasingly indicated for poorly functioning children with intractable epilepsy, because of the minimum risks for disconnection syndrome. The median age at surgery was 7 years in our study, younger than in previous reports. No permanent neurological deterioration was observed postoperatively.

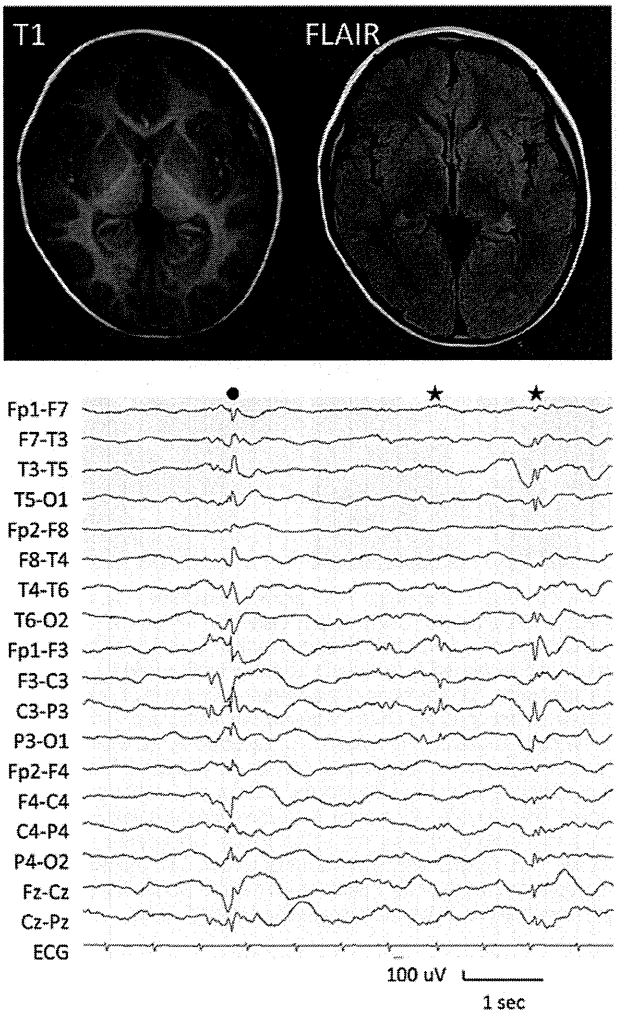

FIG. 1. Case 3. **Upper:** Preoperative T1-weighted and FLAIR MR images showing no abnormalities. **Lower:** Interictal scalp electroencephalogram showing generalized *(filled circle)* and occasional left hemisphere *(stars)* spikes.

In addition to involving a small number of patients, our study is based on relatively short-term follow-up. Since seizure control may change over the years, a longer follow-up study including a larger number of patients is required in the future to validate our results.

Corpus callosotomy may be a more effective treatment option than previously thought for patients with intractable generalized epilepsy and no identified etiology. The majority of our patients had a diagnosis of West syndrome at the onset of epilepsy. West syndrome has been conventionally divided into symptomatic and cryptogenic types. However, to avoid ambiguous use of the term "cryptogenic," a recent population study classified the syndrome into cases with "proven etiology" and those with "no identified etiology."[11,13] Approximately one-third of patients with West syndrome present with no identified etiology.[13] In one retrospective study, 45% of the patients did not respond to first- and second-line therapy, including steroids, vigabatrin, and valproate, and 27% had refractory spasms at the last follow-up examination.[10] Total

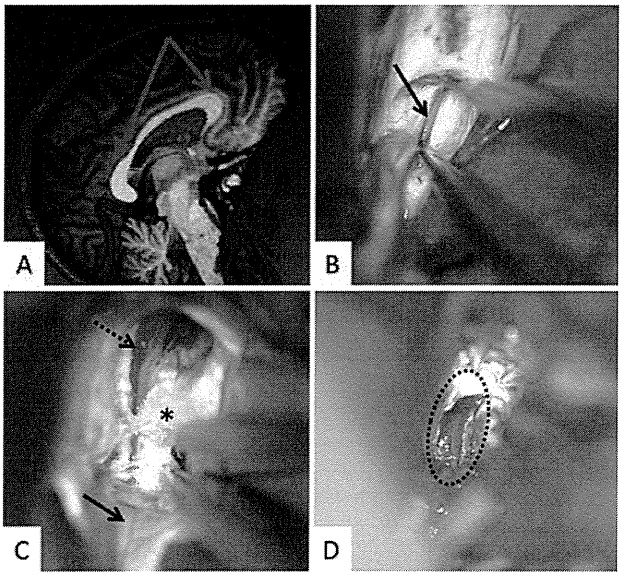

FIG. 2. Case 3. One-stage total corpus callosotomy. **A:** Schematic image of the approach to the corpus callosum *(red arrows)*. Complete callosal section is performed through the right frontal interhemispheric space and advanced to the depth of the operative field by aspirating the splenium. **B:** The body of the corpus callosum is aspirated at the midline to first open the cavity of the septum pellucidum *(arrow)*. Most of the body of the corpus callosum is dissected by following this cavity. **C:** Aspiration of the genu of the corpus callosum. The callosum is aspirated subpially by following the anterior cerebral artery *(dashed arrow)*. The cut plane of the genu is indicated with an *asterisk*. Note that the cavity between the septum pellucidum is fully opened posteriorly *(arrow)*. **D:** Subpial aspiration of the splenium. The procedure is advanced to the depth of the operative field at this stage. The part of the splenium that is aspirated is indicated by a *dotted circle*.

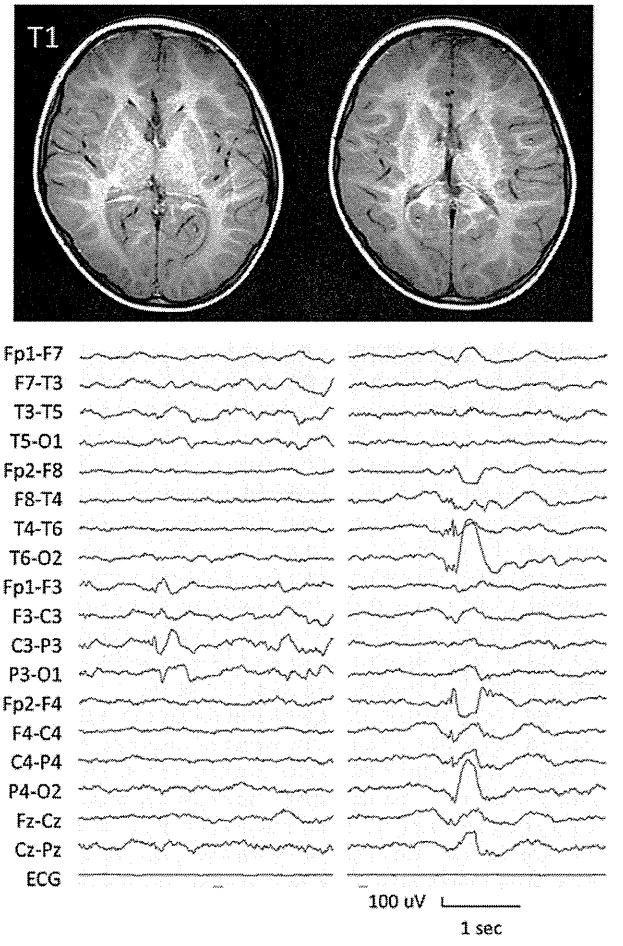

FIG. 3. Case 3. **Upper:** Postoperative T1-weighted MR images showing dissection of the corpus callosum at the midline. **Lower:** Postoperative interictal scalp electroencephalogram showing no generalized spikes. Left and right hemisphere spikes are seen independently.

corpus callosotomy may provide long-term seizure control for such refractory cases with no identified etiology or MRI abnormality. It should be noted that the ketogenic diet and vagus nerve stimulation are less invasive treatment alternatives. A recent study of a pediatric population reported that a greater than 75% reduction in drop attacks was achieved in 43% of patients for 12 months after vagus nerve stimulation.[1] However, complete seizure remission was not described. Corpus callosotomy is probably more effective in terms of seizure control than vagus nerve stimulation, but this increase in effectiveness must be weighed against the increased surgical risks.[15,20]

Complete seizure remission was documented in 0%–10% of patients in larger case series involving corpus callosotomy.[2,16,17] However, those studies focused on "reduction" of seizure frequency, and clinical factors for curative outcome were not investigated. In one recent study, Shim et al.[15] performed 1-stage total corpus callosotomy in 34 patients with pediatric generalized epilepsy (mean age at surgery 8.7 years). A surprisingly high rate of complete seizure freedom (35%) was reported, similar to the findings of our study. However, the authors could not find a clear relationship between MRI findings and outcome. This is probably because of a different patient population. They included mostly symptomatic patients with relatively late onset of epilepsy (mean 2.5 years) and various types of seizures, such as complex partial and generalized tonic-clonic seizures. In contrast, the majority of our patients had earlier onset of epilepsy with electroclinical diagnosis of West syndrome. All of our patients suffered from spasms, axial tonic and atonic seizures, and half of them were considered to have cryptogenic epilepsy.

The present study shows that severing of major corticocortical connections between the hemispheres can dramatically reduce seizures in patients with diffusely distributed epileptogenic cortices. How sectioning of the corpus callosum actually causes complete seizure remission remains unknown. A previous study of callosal electrical potentials showed that the corpus callosum does not simply transfer the epileptic activities from one hemisphere to the other, but rather facilitates simultaneous activation, or synchrony, of epileptic neurons in both hemispheres.[12] Importantly, none of our patients with complete seizure remission had an identifiable seizure etiology. Patients with infantile spasms and no identified etiology form a group with relatively favorable seizure outcome.[13] Thus, the epileptogenic potential is probably lower in those patients. It is important to note that epileptiform discharges were present postoperatively in the electroen-

cephalograms obtained in all of our patients, suggesting that corpus callosotomy itself does not completely suppress epileptic activities. Sectioning of the corpus callosum prevents the development of bisynchronous seizure activities, and in selected cases, a single hemisphere is not sufficient to generate spontaneous seizures, or the seizures can be well controlled by antiepileptic medications.

Conclusions

Complete seizure remission was achieved after total corpus callosotomy in a subgroup of patients with intractable epilepsy subsequent to West syndrome or Lennox-Gastaut syndrome. Corpus callosotomy may be an important treatment option for patients with infantile or early childhood onset epilepsy with unidentified etiology and no MRI abnormalities.

Disclosure

The authors report no conflict of interest concerning the materials or methods used in this study or the findings specified in this paper. Dr. Iwasaki was supported by the Japan Epilepsy Research Foundation. This research was partially supported by Grant-in-Aid for Scientific Research, Japan Society for the Promotion of Science 22791330.

Author contributions to the study and manuscript preparation include the following. Conception and design: Iwasaki, Uematsu, Nakayama, Haginoya, Osawa, Itabashi, Jin, Nakasato. Acquisition of data: Iwasaki, Uematsu, Sato, Nakayama, Haginoya, Itabashi. Analysis and interpretation of data: Iwasaki, Uematsu, Sato, Nakayama, Osawa, Jin, Nakasato, Tominaga. Drafting the article: Iwasaki. Critically revising the article: all authors. Reviewed submitted version of manuscript: all authors. Approved the final version of the manuscript on behalf of all authors: Iwasaki. Study supervision: Uematsu.

References

1. Abd-El-Barr MM, Joseph JR, Schultz R, Edmonds JL, Wilfong AA, Yoshor D: Vagus nerve stimulation for drop attacks in a pediatric population. **Epilepsy Behav 19:**394–399, 2010
2. Cukiert A, Burattini JA, Mariani PP, Câmara RB, Seda L, Baldauf CM, et al: Extended, one-stage callosal section for treatment of refractory secondarily generalized epilepsy in patients with Lennox-Gastaut and Lennox-like syndromes. **Epilepsia 47:**371–374, 2006
3. Iwasaki M, Nakasato N, Kakisaka Y, Kanno A, Uematsu M, Haginoya K, et al: Lateralization of interictal spikes after corpus callosotomy. **Clin Neurophysiol 122:**2121–2127, 2011
4. Jalilian L, Limbrick DD, Steger-May K, Johnston J, Powers AK, Smyth MD: Complete versus anterior two-thirds corpus callosotomy in children: analysis of outcome. Clinical article. **J Neurosurg Pediatr 6:**257–266, 2010
5. Jenssen S, Sperling MR, Tracy JI, Nei M, Joyce L, David G, et al: Corpus callosotomy in refractory idiopathic generalized epilepsy. **Seizure 15:**621–629, 2006
6. Joseph JR, Viswanathan A, Yoshor D: Extraventricular corpus callosotomy. Technical note. **J Neurosurg 114:**1698–1700, 2011
7. Maehara T, Shimizu H: Surgical outcome of corpus callosotomy in patients with drop attacks. **Epilepsia 42:**67–71, 2001
8. Mamelak AN, Barbaro NM, Walker JA, Laxer KD: Corpus callosotomy: a quantitative study of the extent of resection, seizure control, and neuropsychological outcome. **J Neurosurg 79:**688–695, 1993
9. Mathews MS, Linskey ME, Binder DK: William P. van Wagenen and the first corpus callosotomies for epilepsy. Historical vignette. **J Neurosurg 108:**608–613, 2008
10. Mohamed BP, Scott RC, Desai N, Gutta P, Patil S: Seizure outcome in infantile spasms—a retrospective study. **Epilepsia 52:**746–752, 2011
11. O'Callaghan FJK, Lux AL, Darke K, Edwards SW, Hancock E, Johnson AL, et al: The effect of lead time to treatment and of age of onset on developmental outcome at 4 years in infantile spasms: evidence from the United Kingdom Infantile Spasms Study. **Epilepsia 52:**1359–1364, 2011
12. Ono T, Matsuo A, Baba H, Ono K: Is a cortical spike discharge "transferred" to the contralateral cortex via the corpus callosum?: An intraoperative observation of electrocorticogram and callosal compound action potentials. **Epilepsia 43:**1536–1542, 2002
13. Osborne JP, Lux AL, Edwards SW, Hancock E, Johnson AL, Kennedy CR, et al: The underlying etiology of infantile spasms (West syndrome): information from the United Kingdom Infantile Spasms Study (UKISS) on contemporary causes and their classification. **Epilepsia 51:**2168–2174, 2010
14. Pinard JM, Delalande O, Chiron C, Soufflet C, Plouin P, Kim Y, et al: Callosotomy for epilepsy after West syndrome. **Epilepsia 40:**1727–1734, 1999
15. Shim KW, Lee YM, Kim HD, Lee JS, Choi JU, Kim DS: Changing the paradigm of 1-stage total callosotomy for the treatment of pediatric generalized epilepsy. **J Neurosurg Pediatr 2:**29–36, 2008
16. Sunaga S, Shimizu H, Sugano H: Long-term follow-up of seizure outcomes after corpus callosotomy. **Seizure 18:**124–128, 2009
17. Tanriverdi T, Olivier A, Poulin N, Andermann F, Dubeau F: Long-term seizure outcome after corpus callosotomy: a retrospective analysis of 95 patients. Clinical article. **J Neurosurg 110:**332–342, 2009
18. Turanli G, Yalnizoğlu D, Genç-Açikgöz D, Akalan N, Topçu M: Outcome and long term follow-up after corpus callosotomy in childhood onset intractable epilepsy. **Childs Nerv Syst 22:**1322–1327, 2006
19. Wyllie E: Corpus callosotomy for intractable generalized epilepsy. **J Pediatr 113:**255–261, 1988
20. You SJ, Kang HC, Ko TS, Kim HD, Yum MS, Hwang YS, et al: Comparison of corpus callosotomy and vagus nerve stimulation in children with Lennox-Gastaut syndrome. **Brain Dev 30:**195–199, 2008

Manuscript submitted December 7, 2011.
Accepted March 13, 2012.
Please include this information when citing this paper: published online June 8, 2012; DOI: 10.3171/2012.3.PEDS11544.
Address correspondence to: Masaki Iwasaki, M.D., Department of Neurosurgery, Tohoku University Graduate School of Medicine, 1-1 Seiryo-machi, Aoba-ku, Sendai 980-8574, Japan. email: epinetmi@gmail.com.